Studying molecular quantum dynamics with the multiconfiguration time-dependent Hartree (MCTDH) method

Hans-Dieter Meyer[1, *]

[1]*Theoretische Chemie, Universität Heidelberg,*

Im Neuenheimer Feld 229, D-69120 Heidelberg, Germany

(Dated: August 17, 2011)

Abstract

This review covers the multiconfiguration time-dependent Hartree (MCTDH) method, which is a powerful and general algorithm for solving the time-dependent Schrödinger equation. The formal derivation is discussed as well as applications of the method. Recent extensions of MCTDH are treated in brief, namely MCTDHB and MCTDHF, for treating identical particles (bosons and fermions), and the very powerful multi-layer (ML-MCTDH) formalism. Compact representations of potential energy surfaces (PES) are also treated, as the representation of a PES becomes a major bottleneck when going to larger systems (9 or more dimensions) while employing a full dimensional, complicated, and non-separable PES. As applications of MCTDH we discuss the calculation of photo-ionization and photo-excitation spectra of the vibronically coupled systems butatriene and pyrazine, respectively, and the infra-red spectrum of the Zundel cation (protonated water dimer) $H_5O_2^+$.

*Electronic address: Hans-Dieter.Meyer@pci.uni-heidelberg.de

I. INTRODUCTION

Quantum dynamics simulations are an essential tool for understanding experiments which probe matter at an atomic level. Quantum chemistry calculations provide the potential energy surfaces (PES) on which the nuclei of a molecular system move, and this motion is studied by quantum dynamics.

Over the last two decades, there has been an impressive progress in the field of molecular quantum dynamics. A recent review article by Bowman *et. al.*[1] reflects the state of the art of computing vibrational energy levels. See also Refs.[2–5]. But molecular quantum dynamics is much more than computing vibrational energy levels. It also covers inelastic and reactive scattering off molecules or surfaces, the study of intramolecular vibrational energy redistribution (IVR), simulations of pump-probe experiments, control, and more. The computation of vibrational energy levels is still often done by solving the time-independent Schrödinger equation, but for most of the other problems a time-dependent approach has proven to be superior. Even for computing vibrational spectra, the time-dependent approach may be of advantage, namely if there are very many lines such that only an envelope is to be computed or if some high lying states of a larger molecule are of interest. (See the examples discussed in section IV.) For even larger systems, trajectory based quantum methods are an option. The most prominent one of those is the multiple spawning method of Martinez[6].

If the Hamiltonian is time-dependent, e. g. because of an external laser field, the time-dependent version of the Schrödinger equation must be used. For time-independent Hamiltonians, however, time-dependent and time-independent approaches are equivalent. Which approach is to be preferred is largely a matter of numerical efficiency. The time-dependent Schrödinger equation has one variable more, time. On the other hand, the time-dependent equation has a simpler structure, an initial value problem, as compared to the time-independent one, an eigenvalue problem. In a time-dependent approach one is restricted to investigate the properties of an initial state only, whereas a full diagonalization of the Hamiltonian provides one with all information possible. This is actually an advantage of the time-dependent approach because one usually is not interested in all state-to-state transitions (the full S-matrix) and the restriction makes a given problem easier to solve. The last three decades have shown an impressive success of the time-dependent approach[7] to molecular quantum dynamics, in particular when larger molecules are treated.

We note in passing that, after all eigenstates up to a sufficiently high energy are computed, one may expand an initial wave packet in these eigenstates and propagate it by using a well known expression. This has been done (see e. g. Ref.[8]), but only for small systems (up to 4 dimensions, typically), because of the poor scaling of the method. It is one of the main advantages of the time-dependent approach, that eigenstates are avoided.

This article reviews the multiconfiguration time-dependent Hartree (MCTDH) method, which is an efficient algorithm for solving the time-dependent Schrödinger equation (and due to recent developments it can compute eigenstates as well). MCTDH is a complicated algorithm and currently there seem to exist three implementations, the Heidelberg code, the Bielefeld code of Uwe Manthe, and the Las-Cruces code of Haobin Wang. And for the special case of identical particles there are several new codes coming up, MCTDHB ones for bosonic and MCTDHF ones for fermionic systems. In the present article we will discuss the MCTDH algorithm as it is implemented in the Heidelberg code[9], and also the applications discussed are ones performed with the Heidelberg code.

The paper is structured as follows. In the next section we derive the MCTDH equations of motion and discuss their properties. We also briefly discuss extensions of MCTDH, namely MCTDHB, MCTDHF, and ML-MCTDH. The first two are, as already mentioned, for treating indistinguishable particles, whereas the multilayer (ML) extension of MCTDH allows one to tackle very large systems with hundreds or even thousands of degrees of freedom.

In the following section, we discuss potential representations. If there are five atoms (9D) or more, one cannot simply evaluate the potential on all grid-points, there are far too many. One must represent the potential in a compact form which is easy to apply to the wave function. This is a problem which is not unique to MCTDH, it appears for other methods as well where it is known as *quadrature problem*. POTFIT is an algorithm which brings the potential in a compact form similar to the MCTDH wave function. However, POTFIT cannot be used for large product grids and the more approximate n-mode representation, also known as high dimensional model representation (cut-HDMR) or cluster expansion, is therefore discussed as well.

We then turn to applications of MCTDH. First we discuss the calculation of vibronic spectra, namely the photo-ionization spectrum of butatriene and the photo-excitation spectrum of pyrazine. Then, we investigate the infra-red spectrum of the Zundel cation $H_5O_2^+$,

where solving the potential representation problem was a major part of the research. Finally we summarize our findings.

II. MCTDH THEORY

A. The MCTDH equations of motion

The aim is to solve the time-dependent Schrödinger equation

$$i\dot{\Psi} = H\,\Psi \tag{1}$$

(we use a unit system with $\hbar = 1$ throughout). The most straightforward way to solve this equation is to represent the wave function and Hamiltonian in basis set expansions where multi-dimensional basis functions are built from a products of one-dimensional time-independent ones, $\{\chi_j^{(\kappa)}\}$

$$\Psi(q_1,\ldots,q_f,t) = \sum_{j_1=1}^{N_1}\cdots\sum_{j_f=1}^{N_f} C_{j_1\ldots j_f}(t)\prod_{\kappa=1}^{f}\chi_{j_\kappa}^{(\kappa)}(q_\kappa)\,. \tag{2}$$

Here f specifies the number of degrees of freedom, $q_1,\ldots,q_f$ are nuclear coordinates, $C_{j_1\ldots j_f}$ denote time-dependent expansion coefficients, and N_κ is the number of basis functions used for representing the κth degree of freedom (DOF). The resulting method is easy to code and efficient for small systems in particular when a discrete variable representation (DVR)[10,11] is taken as basis, because this makes the representation of the potential energy surface (PES) diagonal. However, this so called *standard method* is plagued by strong exponential scaling as the number of coefficients increases like N^f. This limits the method to smaller problems.

In the MCTDH scheme[12–16] the scaling is softened by introducing an intermediate, smaller, but now time-dependent basis of so-called *single-particle functions* (SPFs). The *ansatz* for the MCTDH-wavefunction reads

$$\begin{aligned}\Psi(q_1,\ldots,q_f,t) &= \sum_{j_1=1}^{n_1}\cdots\sum_{j_f=1}^{n_f} A_{j_1\ldots j_f}(t)\prod_{\kappa=1}^{f}\varphi_{j_\kappa}^{(\kappa)}(q_\kappa,t)\\ &= \sum_J A_J\,\Phi_J\end{aligned} \tag{3}$$

with n_κ usually being considerably smaller than N_κ. Here the configuration, or Hartree-product, Φ_J is an f-dimensional product of SPFs, implicitly defined by Eq. (3). $J =$

$(j_1 \ldots j_f)$ is a composite index, the symbol $A_J \equiv A_{j_1 \ldots j_f}$, often called A-vector, denotes the MCTDH expansion coefficients, and the $\varphi_{j_\kappa}^{(\kappa)}$ are the SPFs, which in turn are represented as linear combinations of the primitive basis

$$\varphi_{j_\kappa}^{(\kappa)}(q_\kappa, t) = \sum_{i_\kappa=1}^{N_\kappa} c_{i_\kappa j_\kappa}^{(\kappa)}(t) \, \chi_{i_\kappa}^{(\kappa)}(q_\kappa) \,. \tag{4}$$

Since both the coefficients and the SPFs are time-dependent, the wave function representation (3) is not unique. Uniquely defined equations of motion (EOM) can be obtained by imposing additional constraints on the SPFs[13–16]. Hereby it can be achieved that initially orthonormal SPFs remain orthonormal for all times. The constraints read

$$\langle \varphi_j^{(\kappa)}(0) | \varphi_l^{(\kappa)}(0) \rangle \; = \; \delta_{jl} \tag{5}$$

$$\langle \varphi_j^{(\kappa)}(t) | \dot{\varphi}_l^{(\kappa)}(t) \rangle \; = \; -i \langle \varphi_j^{(\kappa)}(t) | g^{(\kappa)} | \varphi_l^{(\kappa)}(t) \rangle \,, \tag{6}$$

were $g^{(\kappa)}$ denotes a hermitian but otherwise arbitrary constraint operator. For sake of simplicity we will restrict the discussion here to the simplest and most often used choice $g^{(\kappa)} = 0$.

1. Mean-fields, density matrices and projector

To proceed we introduce *single-hole functions*

$$\Psi_l^{(\kappa)} = \langle \varphi_l^{(\kappa)} | \Psi \rangle = \sum_{J^\kappa} A_{J_l^\kappa} \prod_{\nu \neq \kappa} \varphi_{j_\nu}^{(\nu)} \,, \tag{7}$$

where J_l^κ denotes a composite index J with the κth entry set at l, and J^κ is similar to J but with the κth entry removed. The single-hole functions allow us to write the total wave function as

$$\Psi = \sum_l \varphi_l^{(\kappa)} \Psi_l^{(\kappa)} \tag{8}$$

for any degree of freedom κ. This expansion is used when deriving the equations of motion for the SPFs.

Next we define *mean field*

$$\langle H \rangle_{jl}^{(\kappa)} = \langle \Psi_j^{(\kappa)} | H | \Psi_l^{(\kappa)} \rangle \tag{9}$$

and *density* matrices

$$\rho_{jl}^{(\kappa)} = \langle \Psi_j^{(\kappa)} | \Psi_l^{(\kappa)} \rangle = \sum_{J^\kappa} A_{J_j^\kappa}^* A_{J_l^\kappa} \,. \tag{10}$$

Note that the mean-field matrix elements are operators on the κth DOF. Finally, we define the MCTDH *projector*

$$P^{(\kappa)} = \sum_{j=1}^{n_\kappa} |\varphi_j^{(\kappa)}\rangle\langle\varphi_j^{(\kappa)}|\,,\tag{11}$$

and split the Hamiltonian into separable and correlated terms

$$H = \sum_{\kappa=1}^{f} h^{(\kappa)} + H_{\mathrm{R}}\,,\tag{12}$$

where $h^{(\kappa)}$ acts only on the κth DOF and the residual part, H_{R}, includes all correlations between the DOF.

2. Equations of motion

The MCTDH equations of motion are derived by applying the Dirac-Frenkel variational principle to the *ansatz* Eq. (3). After some algebra one obtains[13,14]

$$i\dot{A}_J = \sum_L \langle\Phi_J|H|\Phi_L\rangle A_L\,,\tag{13}$$

$$\dot{\varphi}_j^{(\kappa)} = \left(1 - P^{(\kappa)}\right)\left[h^{(\kappa)}\varphi_j^{(\kappa)} + \sum_{k,l}\left(\boldsymbol{\rho}^{(\kappa)^{-1}}\right)_{jk}\langle H_R\rangle_{kl}^{(\kappa)}\varphi_l^{(\kappa)}\right]\,.\tag{14}$$

The MCTDH equations conserve the norm and, for time-independent Hamiltonians, the total energy. This follows directly from the variational principle[14]. MCTDH contains Time-Dependent Hartree (TDH) and the standard method as limiting cases. MCTDH simplifies to TDH when setting all $n_\kappa = 1$. Increasing n_κ recovers more and more correlation, until finally, for $n_\kappa = N_\kappa$, the standard method is used.

Diagonalizing the matrix $\boldsymbol{\rho}^{(\kappa)}$ yields the *natural populations* and *natural orbitals*[12–14]. The first are defined as the eigenvalues of $\boldsymbol{\rho}^{(\kappa)}$ and the latter are obtained by transforming the SPFs with the eigenvector matrix of $\boldsymbol{\rho}^{(\kappa)}$. Natural populations are a measure of the contribution of the related natural orbitals to the representation of the wave function. Small natural populations indicate that the MCTDH expansion converges, and this provides an important internal check on the quality of the computed solution. For vanishing eigenvalues, the hermitian and positive semi-definite density matrix will become singular. How to solve the resulting numerical problem is discussed in Refs.[13,14].

The EOMs (13,14) are a set of non-linear coupled differential equations. Note that $\dot{A}$ depends on φ through the matrix elements of H and $\dot{\varphi}$ depends on A through the mean fields. One may use an all purpose numerical integration scheme (e. g. Adams-Bashfort-Moulton predictor-corrector, Runge-Kutta, etc.) to solve these equations. However, to speed up the integration a special dedicated integration scheme has been developed, the so called *constant mean field* (CMF) integration scheme[14,16–18].

3. Electronic states

The motion of the molecular nuclei may not evolve on a single Born-Oppenheimer potential energy surface, and a multi-state formulation may be necessary. The MCTDH algorithm can be applied straightforwardly to systems where more than one electronic state is included. One simply chooses one extra DOF, the κ_eth say, to represent the electronic manifold[19]. The coordinate q_{κ_e} then labels the electronic states, taking only discrete values $q_{\kappa_e} = 1, 2, \ldots, \sigma$, where σ is the number of electronic states under consideration. The number of single-particle functions for such an electronic mode is set to the number of states, i.e. $n_{\kappa_e} = \sigma$. The equations of motion (13,14) remain unchanged, treating nuclear and electronic modes on the same footing. This is called the *single-set formulation*, since only one set of SPFs is used for all electronic states.

Because the motion on the included electronic potential energy surfaces can be vastly different, one may think of more efficient ways to include electronic states. The so-called *multi-set formulation* employs different sets of SPFs for each electronic state[20,21]. In this formulation the wave function Ψ is expanded in a set, $\{|\alpha\rangle\}$, of electronic states:

$$|\Psi\rangle = \sum_{\alpha=1}^{\sigma} \Psi^{(\alpha)} |\alpha\rangle \tag{15}$$

where each state function $\Psi^{(\alpha)}$ is expanded in MCTDH form (3). The derivation of the equations of motion is similar to above, except that extra state labels are introduced on the various quantities such as mean fields and density matrices. For details see Refs.[14,20,21]. The single-set formalism is of advantage if the dynamics in the different electronic states is similar, e. g. when the surfaces are almost parallel. The more complicated multi-set formalism is more efficient when the dynamics on the various diabatic states is rather different. In most cases multi-set is the preferred scheme.

B.   MCTDHB and MCTDHF generalizations of MCTDH

The MCTDH method does not take into account particle exchange symmetry, it treats all nuclei as distinguishable. However, when turning to investigate the dynamics of identical particles, bosons or fermions, the particle exchange symmetry must be included. To simplify the discussion, we assume in the following one dimensional spin-polarized particles. Hence the number of particles is identical to the number of DOF, f. As the exchange symmetry is between particles and not among DOF, one needs mode combination to describe two- or three-dimensional identical particles within MCTDH. Mode combination will be discussed in the following section.

As now all particles are identical they must be described by an identical set of SPFs. Hence one needs to propagate only one set of SPFs and the index κ is to be dropped from Eq. (14). To arrive at a fully (anti-) symmetric wave function, the A-vector has to be (anti-) symmetrized, i. e. $A_{j_1 \ldots j_f}$ remains unchanged (changes sign) when two of its indices are interchanged. As the Hamiltonian is symmetric, an initially (anti-) symmetrized wave function keeps its symmetry during propagation. In fact, a loss of symmetry is an indication that the number of SPFs included in the calculation is too small. With this simple symmetrization scheme, implemented in the Heidelberg MCTDH package[9], a couple of small but highly correlated bosonic systems was successfully investigated[22–26].

More powerful algorithms and codes can be obtained by re-deriving MCTDH for identical particles from scratch. This leads to the MCTDHB (MCTDH for bosons) and MCTDHF (MCTDH for fermions) methods. The starting point is a slight modification of the *ansatz* Eq. (3) which we write compactly as

$$\Psi(q_1, \ldots, q_f, t) = \sum_J A_J(t) \, \Phi_J(q_1, \ldots, q_f, t) \tag{16}$$

In contrast to Eq. (3) the configurations Φ_J are no longer Hartree products but symmetrized products, so called permanents, or anti-symmetrized products, the well known Slater determinants. Among others, this shortens the length of the A-vector. The number of configurations is n^f for distinguishable particles, but

$$\binom{f+n-1}{f} = \frac{(f+n-1)!}{f! \, (n-1)!} \tag{17}$$

8

for bosons and

$$\binom{n}{f} = \frac{n!}{f!\,(n-f)!} \tag{18}$$

for fermions. Note that for fermionic systems the number of SPFs, n, must not be smaller than the number of particles, f. For $n = f$ MCTDHF turns into Hartree-Fock. Similarly, for $n = 1$ MCTDHB becomes equivalent to the Gross-Pitaevskii approach[27,28].

The equations of motion remain virtually unchanged. The A-vector is still propagated according to Eq. (13), but the evaluation of the Hamiltonian matrix elements is changed as Φ is now a permanent or determinant. Similarly, the EOM for the SPFs is still given by Eq. (14) but with the modification that there is only one set of SPFs, i. e. there is no longer an index κ.

The Hamiltonian of bosonic and fermionic systems is often determined by one- and two-body forces alone

$$H = \sum_{i=1}^{f} h(q_i) + \sum_{i<j}^{f} W(q_i, q_j) \tag{19}$$

where h denotes the sum of one-particle kinetic energy and a one-particle interaction potential, e. g. a confining potential. The two-particle potential, denoted by W, is usually a Feynman contact potential (δ-interaction) or a Coulomb potential. This special form of the interaction allows to write the mean-field (Eq. (9)) slightly more explicit, leading to the EOM[29]

$$i\dot{\varphi}_j = (1 - P)\left[h\varphi_j + \sum_{klrs}\{\boldsymbol{\rho}^{-1}\}_{jk}\,\rho_{klrs}\,W_{lr}\,\varphi_s\right]\,, \tag{20}$$

where

$$W_{lr}(q, t) = \int \varphi_l^*(q', t)W(q, q')\varphi_r(q', t)dq' \,. \tag{21}$$

The symbol ρ_{klrs} denotes a two-particle density.

Derivation of the MCTDHB method and applications of this method are discussed in Refs.[29–32]. The MCTDHF method was developed by three groups independently[33–35]. MCTDHF has been used to solve problems of quantum chemistry[35,36], but most applications of MCTDHF deal with molecules in strong laser fields[33,37–39]. The nuclear geometry is kept frozen but the electrons driven by the laser field travel large distances. Very recently an approach was developed to treat nuclear and electronic motion simultaneously by an extension of MCTDHF[40]. Ionization of diatoms was studied with this new approach.

C.   Mode combination

Although MCTDH can treat larger systems than the standard method, Eq. (2), it still shows an exponential scaling with the number of DOF. The base of exponentiation, however, is reduced from N to n because the two methods scale like n^f and N^f, respectively. The base can be further reduced by introducing an algorithm called mode combination. The SPFs do not need to depend on a single DOF, they may as well depend on a collection of DOF. To this end we introduce combined coordinates, also called logical coordinates or particles,

$$Q_\kappa = \{q_{1,\kappa}, \cdots, q_{d_\kappa,\kappa}\} \tag{22}$$

where κ now runs over the particles and the κth particle (logical coordinate) consists of d_κ physical coordinates. The *ansatz* for the wave function is virtually unchanged, except for expanding the wave function now in multi-dimensional SPFs

$$\Psi(q_1,\ldots,q_f,t) \equiv \Psi(Q_1,\ldots,Q_p,t) = \sum_{j_1=1}^{n_1} \cdots \sum_{j_p=1}^{n_p} A_{j_1\ldots j_p}(t) \prod_{\kappa=1}^{p} \varphi_{j_\kappa}^{(\kappa)}(Q_\kappa,t) \tag{23}$$

where p denotes the number of particles. The equations of motion (13,14) remain unchanged except for replacing the number of DOF, f, with the number of particles, p. Note that the operators $h^{(\kappa)}$ operate now on particles (combined modes) rather than on DOF.

Mode combination leads to a considerably shorter A-vector but the SPFs are now represented in multi-dimensional primitive product basis sets (or DVR-grids) and thus harder to propagate. Typical choices for the degree of contraction are $d=1$, 2, or 3. Higher order contractions are rare because they make the propagation of the SPFs too elaborate.

The effect of mode combination can be very substantial. To understand this let us discuss how much data is needed to represent one wave function. Fewer data leads, of course, to less memory consumption. But the CPU-time also depends on how much data is needed to represent one wave function, because this amount of data must be processed at each time step of the propagation.

Let us assume, for sake of simplicity, that all DOF have same grid length N and numbers of SPFs n. Then a wave function in standard method format takes N^f data points, and an MCTDH wave function takes $fnN + n^f$ data points, where the first summand counts the data needed to represent the SPFs and the second stands for the A-vector. With mode combination the latter equation turns into $p\tilde{n}\tilde{N} + \tilde{n}^p$, where a tilde is added to N and n

to distinguish particle grid sizes from one-dimensional ones and similar for the numbers of SPFs. (We will drop the tilde later, if no confusion is possible.) Obviously $\tilde{N} = N^d$, but there is no strict rule how $\tilde{n}$ scales, this depends on the case. However, the estimate $\tilde{n} = dn$ was found useful as a rule of thumb. An example shall demonstrate the importance of mode combination. Let us assume that there are $f = 15$ DOF, $N = 16$ grid points and $n = 5$ SPFs for each DOF. A standard method wave function then takes 1.15×10^{18} data points, MCTDH without mode combination 3.05×10^{10}, and MCTDH with combining always three DOF, i. e. $d = 3$, $p = 4$, and using $\tilde{n} = 15$, takes 1.07×10^6 data points. The first problem is clearly infeasible, straight MCTDH would require a super-computer to solve this problem, but MCTDH with mode combination is easily doable on a normal PC. Note that the base of the exponentially scaling part drops from N to n to $\tilde{n}^{(1/d)}$ in general, or from 16 to 5 to 2.5 for our example.

The number of SPFs needed for convergence depends on the combination scheme and the question which DOF should be combined to build a particle is a delicate one. One should combine those DOF between which a strong coupling exists. Then their correlation is treated on the SPF level and does not appear in the configuration interaction part leading to fewer SPFs and hence to a shorter A-vector. A more technical rule states that all particle grids should have roughly the same size. Too large particle sizes must be avoided, because if one over-combines such that the propagation of the SPFs becomes the major part of the total effort, the MCTDH propagation becomes less efficient. As a rule of thumb, the number of data points needed to represent the SPFs should be smaller than the A-vector, i. e. $p\tilde{n}\tilde{N} < \tilde{n}^p$.

D.   Multi-layer MCTDH

The introduction of mode combination was a very important step when going to larger systems. But the exponential increase of the particle grid with the combination order d limits the combination order in general to 3, and in suitable cases (small DOF-grids) to 4 or 5. However, we know a method to efficiently propagate multi-dimensional wave functions: MCTDH! Hence one may use MCTDH rather than the standard method to propagate the SPFs of an MCTDH calculation. And one can go on and use again MCTDH to propagate the SPFs of the set of secondary MCTDH calculations, and so on. This is the general idea

of the multi-layer MCTDH (ML-MCTDH) approach. ML-MCTDH was first formulated and implemented by Wang and Thoss[41] (see also Ref.[15] where this approach is called *cascading*). The ML-MCTDH algorithm was re-formulated by Manthe[42,43] in a recursive way, which allows to treat an arbitrary number of layers. This recursive formulation was used to implement[44] ML-MCTDH in the Heidelberg MCTDH package[9].

The ML-MCTDH equations of motion are essentially those of MCTDH, i. e. an equation similar to (14) applies to all SPFs of all layers, but the specific form of projector, density matrix, and mean-field depends on the particular layer. In detail the equations are very cumbersome because several additional indices are needed to specify the layer and the path through the ML-tree. We refer the interested reader to Refs.[42,44].

An ML-MCTDH tree is an extension of an MCTDH mode combination scheme. A graphical representation[42] of the tree is illuminating. Fig. 1 shows a collection of trees. A circle stands for a set of coefficients (A-vector(s)) and a square for a set of (time-independent) primitive basis functions (or DVR grids). A standard method tree is shown in Fig. 1a. Here the primitive basis functions are directly connected with the coefficients (see Eq.(2)). Fig. 1b displays an MCTDH tree. The uppermost circle stands for the A-vector which is connected to the coefficient vectors (see Eq. (4)) of the SPFs, which in turn are connected to the primitive basis sets. Fig. 1c shows a tree for an MCTDH calculation with mode combination. Here the SPFs depend on more than one DOF (two in the present example). Fig. 1d shows an ML-MCTDH tree. The uppermost SPFs (second level) are expanded into the SPFs of the following layer (third level) which in turn are expanded in the primitive basis sets. We call this a three-layer calculation because the circles appear on three different levels. MCTDH is thus a two-layer calculation and the standard method a one-layer one. ML-MCTDH can have more layers than three and can be used together with mode combination. An example of such a case is displayed in Fig. 1e. For the construction of a tree similar rules apply as for constructing a combination scheme (see above).

MCTDH is very efficient if the modes are not particular strongly correlated. Then a small number of SPFs suffices for convergence. Moreover, MCTDH is very fast if a high accuracy is not envisaged. But MCTDH becomes costly if very accurate results are desired as then many SPFs are needed. ML-MCTDH is MCTDH to the extreme. It can be amazingly fast if one can tolerate small errors but a highly accurate convergence is difficult to achieve. A careful analysis of the convergence properties of ML-MCTDH is provided in Ref.[44] and a
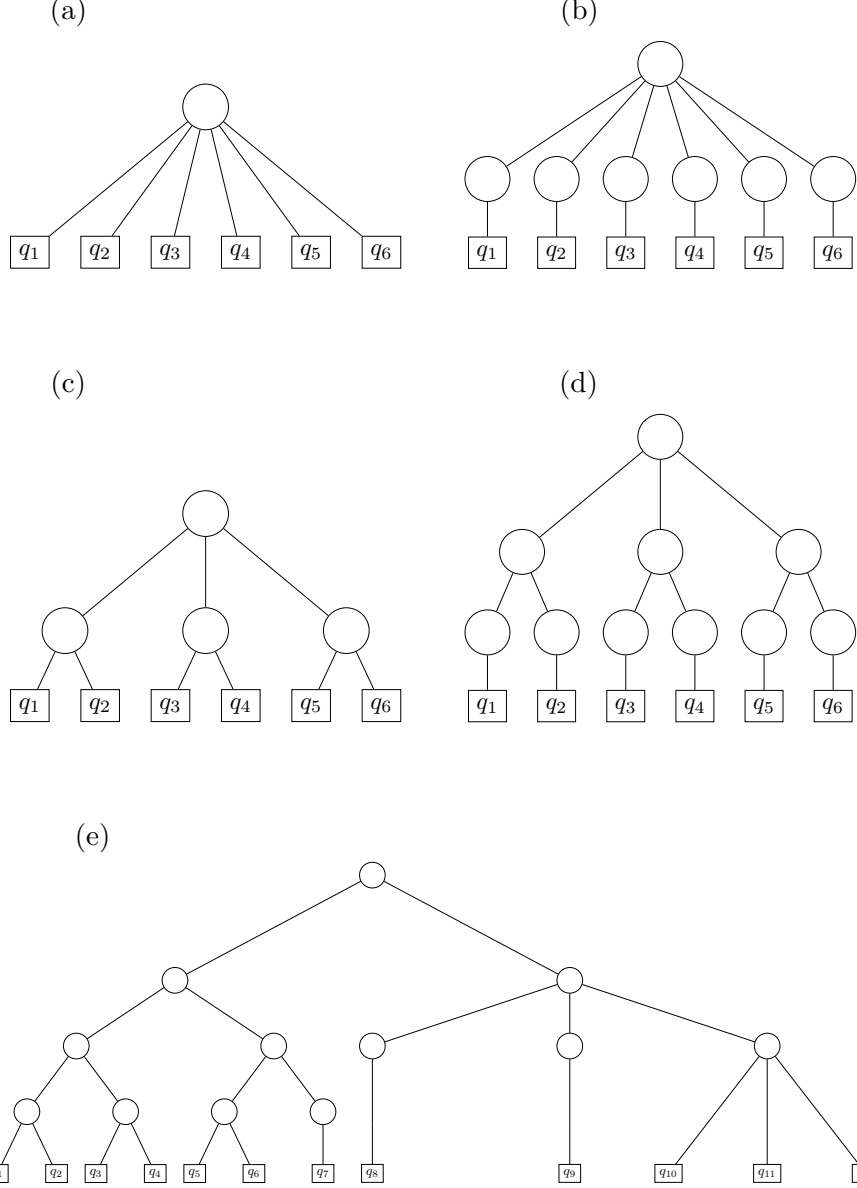
FIG. 1: Tree structures of wave functions. (a) Standard method wave function tree, where the wave function is expanded directly into a primitive (time-independent) basis denoted by squares. The circle symbolizes the expansion coefficients. (b) MCTDH wave function tree where the wavefunction is first expanded into a basis of SPFs, which, in turn, are expanded into the primitive basis. (c) MCTDH with mode combinations. The SPFs are expanded in two-dimensional primitive basis sets. (d) ML-MCTDH wave function tree. The (two-dimensional) SPFs of the second layer are expanded into (one-dimensional) SPFs of the third layer which in turn are expanded into the primitive basis. This case is similar to case (c), except that an additional layer is introduced rather than using combined primitives. (e) ML-MCTDH wave function tree with three and four layers and with mode combination.

13

demonstration of the efficiency of ML-MCTDH is given in section IV A when discussing the pyrazine example. The most impressive ML-MCTDH calculations to date, including up to several thousands of degrees of freedom, are discussed by Wang and Thoss[45–51]. The latter applications are of system/bath type. A small system interacts with a (often harmonic) bath of thousands of degrees of freedom. The interaction with a single bath mode is rather weak, but the interaction of the system with the bath as total is strong. Such problems are very suitable for ML-MCTDH.

The grouping of modes on which mode combination and ML-MCTDH relies is incompatible with (anti-)symmetrization. Hence ML-MCTDH cannot treat identical particles, e. g. electrons. To overcome this limitation Wang and Thoss have developed[52] an alternative MCTDH *ansatz* which is based on second quantization. As creation/annihilation operators can be grouped, this *ansatz* allows for an ML extension.

E. Relaxation and improved Relaxation

The generation of a ground–state wavefunction is conveniently done by energy relaxation[53]. An initial wave packet, often a Hartree product, is propagated in negative imaginary time by $H - E(t)$, where $E(t)$ denotes the expectation value of H.

$$\dot{\Psi} = -(H - E(t))\Psi \quad \text{with} \quad E(t) = \langle \Psi(t) | H | \Psi(t) \rangle . \tag{24}$$

The energy E can be interpreted as a Lagrange parameter introduced to keep the norm of Ψ constant (we assume Ψ to be normalized). One may drop $E(t)$ from the differential equation and re-normalize Ψ periodically. Differentiation of $E(t)$ leads to

$$\dot{E} = -\langle \Psi(t) | (H - E(t))^2 | \Psi(t) \rangle . \tag{25}$$

Hence the energy decreases with relaxation time and converges if the variance vanishes, i. e. if the wave function becomes an eigenstate of H. Usually this will be the ground state, only if the initial state is orthogonal to the ground state the algorithm may converge to an excited state.

Relaxation works well if the initial state Ψ has a reasonable overlap with the ground state and if the ground state is well separated. However, relaxation may converge slowly if the energy of the first excited state, E_1, is close to the ground state energy E_0. To damp

out the contributions from the first excited state a relaxation time of about $20/(E_1 - E_0)$ is required. (Note 1 eV $\cdot$ 1 fs $= 1.519\hbar$).

The relaxation can be accelerated and excited states can be computed as well, if the MCTDH A-vector is not determined by relaxation but by diagonalization. This variant is called *improved relaxation*[54]. The algorithm can be derived via a standard time-independent variational principle $\delta\{\langle\Psi|H|\Psi\rangle - \text{constraints}\} = 0$, i. e.

$$\delta\big\{\langle\Psi|H|\Psi\rangle - E\big(\sum_J A_J^* \, A_J - 1\big) - \sum_{\kappa=1}^{f}\sum_{j,l=1}^{n_\kappa} \epsilon_{jl}^{(\kappa)}\big(\langle\varphi_j^{(\kappa)}|\varphi_l^{(\kappa)}\rangle - \delta_{jl}\big)\big\} = 0 \qquad (26)$$

The first Lagrange parameter, E, ensures that the A-vector is normalized and the $\epsilon_{jl}^{(\kappa)}$ ensures that the SPFs are orthonormal. *Improved relaxation* may be viewed as a vibrational MCSCF procedure. Other MCSCF approaches to solve the molecular vibrational problem are discussed in Refs.[2,55–57].

Varying A_J^* yields

$$\sum_K H_{JK} \, A_K = E \, A_J \qquad (27)$$

Hence the coefficient vector is obtained as an eigenvector of the Hamiltonian matrix represented in the basis of the SPFs. And a variation with respect to $\varphi_j^{(\kappa)*}$ yields[54,58]

$$\sum_{l=1}^{n_\kappa} \langle H\rangle_{jl}^{(\kappa)} \, \varphi_l^{(\kappa)} = \sum_{l=1}^{n_\kappa} \epsilon_{jl}^{(\kappa)} \, \varphi_l^{(\kappa)} \qquad (28)$$

This equation can be re-formulated as

$$-\big(1 - P^{(\kappa)}\big) \sum_{k,l} \big(\boldsymbol{\rho}^{(\kappa)^{-1}}\big)_{jk} \langle H\rangle_{kl}^{(\kappa)} \, \varphi_l^{(\kappa)} = 0 \qquad (29)$$

and one notices that the left hand side is the derivative of an SPF in negative imaginary time, $\partial\varphi_j/\partial\tau$ with $\tau = -it$. (Compare with Eq. (14). The splitting of H into a separable and residual part can be done here as well.) This suggests that one can obtain the updated SPFs simply by relaxation. In fact, one can show that

$$\dot{E} = -2\sum_{\kappa=1}^{f}\sum_{l=1}^{n_\kappa} \|\sum_{j=1}^{n_\kappa} \big(\boldsymbol{\rho}^{(\kappa)^{1/2}}\big)_{lj} \, \dot{\varphi}_j^{(\kappa)}\|^2 \leq 0 \qquad (30)$$

holds during relaxation of the SPFs[15,16,54]. Hence, SPF relaxation will always lower the energy. As the energy cannot decrease indefinitely, the time derivative of the SPFs must vanish for $\tau \to \infty$ and Eq. (29) is satisfied for sufficiently long relaxation times.

15

Improved relaxation proceeds as follows: At first an initial state has to be defined. This state should have a reasonable overlap with the sought state. Then the matrix representation of the Hamiltonian H_{JK} is built and diagonalized by a Davidson routine[59,122]. Then the mean-fields are built and the SPFs are relaxed. After that, H_{JK} is re-built in the space of the new SPFs and so on till convergence. If the ground state is computed, the selection of the eigenvector of the Hamiltonian matrix is simple: one takes the eigenvector of lowest energy. When excited states are to be computed, that eigenvector is taken which corresponds to the wavefunction which has the largest overlap with the initial state.

An MCTDH propagation always works, whatever the numbers of SPFs. If there are too few configurations, the propagation will be less accurate but usually still describes the overall features rather well. This is in contrast to *improved relaxation* which fails to converge when the configuration space is too small. There is never a problem in computing the ground state, but converging to excited states becomes more difficult the higher the excitation energy, or, more precisely, the higher the density of states.

The *improved relaxation* algorithm may be used in block form[1,60], i. e. one may start with a block of initial vectors which then converge collectively to a set of eigenstates. Formally the different wave functions are treated as electronic states of one 'super wavefunction'. As the single-set algorithm is used, there is one set of SPFs for all wave functions. The mean-fields are hence state-averaged mean-fields and the Davidson routine is replaced by a block-Davidson one. The block form of *improved relaxation* is more efficient than the single vector one when several eigenstates are to be computed. However, the block form requires considerably more memory.

Improved relaxation has been applied quite successfully to a number of problems, see e. g. Refs.[54,60–62]. For 4-atom systems (6D) it is in general possible to compute all eigenstates of interest. For a system as large as $H_5O_2^+$ (15D) it was, of course, only possible to converge low-lying states[62].

III. REPRESENTATIONS OF THE POTENTIAL ENERGY SURFACE

A. The product form

The set-up of Hamiltonian matrix and mean-fields can become a major part of the MCTDH work to be performed. Multi-dimensional integrals have to be done at every time-step and these integrals are difficult to perform. A fast algorithm for evaluating the integrals is needed, otherwise MCTDH cannot be competitive. But this problem is not a problem of MCTDH alone, it applies to most other quantum dynamical methods, e. g. vibrational configuration interaction (VCI)[1,63,64], as well. If there are $f = 6$ or more DOFs, the evaluation of the matrix elements $\langle \Phi_J | H | \Phi_L \rangle$, where Φ_J denotes a configuration, becomes very time consuming (if not impossible), even though they have to be done only once for time-independent methods. This difficulty is known as *quadrature problem*.

The computation of the Hamiltonian matrix elements is substantially simplified if the Hamiltonian is of product form, i. e. if it can be written as

$$H = \sum_{r=1}^{s} c_r \prod_{\kappa=1}^{f} h_r^{(\kappa)} \quad , \tag{31}$$

where $h_r^{(\kappa)}$ operates on the κth DOF only and where c_r is a number. Then multi-dimensional integrals can be written as a sum of products of one-dimensional integrals,

$$\langle \Phi_J | H | \Phi_L \rangle = \sum_{r=1}^{s} c_r \langle \varphi_{j_1}^{(1)} | h_r^{(1)} | \varphi_{l_1}^{(1)} \rangle \dots \langle \varphi_{j_f}^{(f)} | h_r^{(f)} | \varphi_{l_f}^{(f)} \rangle \quad , \tag{32}$$

where the configuration Φ and the composite index J are defined after Eq. (3). An equation similar to (32) applies to the mean-fields.

As one-dimensional integrals are done very fast, the computation of the Hamilton matrix elements according to Eq. (32) is much faster than performing multi-dimensional integrals directly. Storage requirements are also much smaller. Fortunately, kinetic energy operators (KEO) are often of product form, and when polyspherical coordinates[65] are used, a product form of the KEO is ensured. The potential energy surface (PES), however, is often not of product form, although a polynomial fit of the potential – when done in the same coordinates as the dynamical calculation – is of desired product form. (Such a polynomial fit was used for e. g. the HONO potential[66,67].) Finally, model Hamiltonians are often of product form. In the following we will discuss a method, called *POTFIT*[14,68,69], which allows to transform

a general PES to product form, while controlling the error which is introduced by this re-fitting procedure.

B.   The POTFIT algorithm

We assume that a global full dimensional PES exists for the problem under discussion. We are not concerned with the problem of fitting a global *ansatz* to *ab initio* points, we assume that this has been done. Our concern is the transformation of a general PES to product form.

A direct way to product form is an expansion of the PES in a product basis. Hence we approximate some given potential V by

$$V^{\mathrm{app}}(q_1,\ldots,q_f) = \sum_{j_1=1}^{m_1} \ldots \sum_{j_f=1}^{m_p} C_{j_1\ldots j_f}\, v_{j_1}^{(1)}(q_1)\ldots v_{j_f}^{(f)}(q_f)) \ . \tag{33}$$

The basis functions $v_{j_\kappa}^{(\kappa)}$ are called *single-particle potentials* (SPP). The expansion orders, m_κ, must be chosen large enough to achieve an accurate expansion. On the other hand they should be as small as possible, because the numerical effort of the integral calculation scales linearly with the number of potential terms, i. e. with the product of the expansion orders. Hence both the expansion coefficients and the SPPs should be optimized to provide the best approximate potential for a given set of expansion orders.

Before we turn to analyze this optimization problem, we simplify it somewhat. When DVRs are used to represent the wave functions, one needs to know the potential only at grid points. This allows us to work in finite dimensional discrete vector spaces. The full potential is now represented as a tensor

$$V_{i_1\ldots i_f} = V\big(q_{i_1}^{(1)},\ldots,q_{i_f}^{(f)}\big) \ , \tag{34}$$

where $q_i^{(\kappa)}$ denotes the coordinate of the ith grid point of the κth grid. The approximate tensor is written as

$$V_{i_1\ldots i_f}^{\mathrm{app}} = \sum_{j_1=1}^{m_1} \ldots \sum_{j_f=1}^{m_f} C_{j_1\ldots j_f}\, v_{i_1 j_1}^{(1)} \ldots v_{i_f j_f}^{(f)} \ , \tag{35}$$

with $v_{ij}^{(\kappa)} = v_j^{(\kappa)}(q_i^{(\kappa)})$. The SPPs are assumed to be orthonormal on the grid, $\sum_i v_{ij}^{(\kappa)} v_{il}^{(\kappa)} = \delta_{jl}$. Throughout this section we will use the letters i and k to label grid points and j and

l to label SPPs. In the mathematical literature the expansion (35) is known as Tucker format[70,71].

The task is now to determine optimal coefficients and SPPs. To this end we minimize

$$\Delta^2 = \sum_{i_1=1}^{N_1} \cdots \sum_{i_f=1}^{N_f} \left(V_{i_1 \ldots i_f} - V_{i_1 \ldots i_f}^{\mathrm{app}} \right)^2 = \sum_I (V_I - V_I^{\mathrm{app}})^2 \quad , \tag{36}$$

where I denotes a composite index which runs over all grid points. Minimizing Δ^2 by varying only the coefficients yields

$$C_{j_1 \ldots j_f} = \sum_{i_1=1}^{N_1} \cdots \sum_{i_f=1}^{N_f} V_{i_1 \ldots i_f} \, v_{i_1 j_1}^{(1)} \cdots v_{i_f j_f}^{(f)} \quad , \tag{37}$$

i. e. the coefficients are given by overlap.

More difficult is to find optimal SPPs. Within POTFIT one defines the SPPs as eigenvectors of the potential density matrices

$$\varrho_{kk'}^{(\kappa)} = \sum_{I^\kappa} V_{i_1 \ldots i_{\kappa-1} k i_{\kappa+1} \ldots i_f} \, V_{i_1 \ldots i_{\kappa-1} k' i_{\kappa+1} \ldots i_f} = \sum_{I^\kappa} V_{I_k^\kappa} V_{I_{k'}^\kappa} \quad , \tag{38}$$

where similar to above I^κ denotes a composite index which contains all grid indices except the κth one, and in I_k^κ the κth entry is replaced by k. The eigenvectors are ordered according to their eigenvalues (largest comes first), i. e. one neglects SPPs with small eigenvalue and hence small contribution to the potential. This approach is known to be optimal for the two-dimensional case[72]. For the general f-dimensional case ($f>2$), POTFIT is not optimal but provides SPPs which are close enough to optimal ones to be useful. Fully optimal SPPs can be found – in principle – by minimizing Δ^2, Eq. (36), with the aid of a general minimization procedure, e. g. simulated annealing or genetic algorithm. But such procedures are much too costly.

1. Contraction over one degree of freedom

The number of expansion terms, $s = \prod_{\kappa=1}^{f} m_\kappa$ appearing in Eq. (35), should be as small as possible, because this number determines the effort of the integral calculation using this product-form potential. At virtually no cost one can reduce the number of expansion terms by one expansion order m_ν, where ν denotes the DOF over which a contraction is performed.

To this end we define *contracted expansion coefficients*

$$D^{(\nu)}_{j_1...j_{\nu-1}i_\nu j_{\nu+1}...j_f} = \sum_{j_\nu=1}^{m_\nu} C_{j_1...j_f} \, v^{(\nu)}_{i_\nu j_\nu} \quad . \tag{39}$$

As the expansion order m_ν will no longer appear in the working equation for V^{app}, one may set $m_\nu = N_\nu$ and use the full set of SPPs for this particular DOF. In this case one performs a unitary transformation on the νth index of the potential to obtain the coefficient C, and then performs the inverse unitary transformation on the νth index of the coefficient. Hence effectively there is no transformation on the νth index and $D^{(\nu)}$ is conveniently computed as

$$D^{(\nu)}_{j_1...j_{\nu-1}i_\nu j_{\nu+1}...j_f} = \sum_{I^\nu} V_{i_1...i_f} \, v^{(1)}_{i_1 j_1} \cdots v^{(\nu-1)}_{i_{\nu-1} j_{\nu-1}} \, v^{(\nu+1)}_{i_{\nu+1} j_{\nu+1}} \cdots v^{(f)}_{i_f j_f} \quad . \tag{40}$$

Note that the νth potential density matrix and the C-tensor are no longer needed. Using contraction, the approximate potential is written as

$$V^{\text{app}}_{i_1...i_p} = \sum_{j_1=1}^{m_1} \cdots \sum_{j_{\nu-1}=1}^{m_{\nu-1}} \sum_{j_{\nu+1}=1}^{m_{\nu+1}} \cdots \sum_{j_p=1}^{m_p} D^{(\nu)}_{j_1...j_{\nu-1}i_\nu j_{\nu+1}...j_p}$$
$$\times v^{(1)}_{i_1 j_1} \cdots v^{(\nu-1)}_{i_{\nu-1} j_{\nu-1}} v^{(\nu+1)}_{i_{\nu+1} j_{\nu+1}} \cdots v^{(f)}_{i_f j_f} \quad . \tag{41}$$

Contraction over the νth DOF is a very helpful trick as it substantially reduces the numerical effort of the following integral evaluation without affecting the accuracy of the product expansion. One should contract over that DOF which otherwise would require the largest expansion order.

2. *Error estimate*

Although the POTFIT algorithm does not provide a fully optimal product form (except for $f = 2$), it is sufficiently close to optimal to be very useful. This is shown by the following error-bound formula.

$$\frac{\Lambda}{f-1} \leq \Delta^2_{opt} \leq \Delta^2 \leq \Lambda \quad \text{with} \quad \Lambda = \sum_{\substack{\kappa=1 \\ \kappa \neq \nu}}^{f} \sum_{j=m_\kappa+1}^{N_\kappa} \lambda^{(\kappa)}_j \quad . \tag{42}$$

Here $\lambda^{(\kappa)}_j$ denotes the jth eigenvalue of the potential-density matrix $\varrho^{(\kappa)}$, ν denotes the contracted DOF, and Δ^2_{opt} is the optimal L^2 error, i. e. the one obtained when the SPPs are truly optimized. Obviously, Λ is the sum of the natural weights of neglected SPPs. The

L^2 error, Δ^2, is rigorously bounded by this sum. If all SPPs are included, i. e. if $m_\kappa = N_\kappa$, POTFIT reproduces the original potential *exactly* on the grid points. Moreover, the last inequality of Eq. (42) tells one how to choose the expansion orders, m_κ, for a given error to be tolerated. The inequality in the middle is trivial, but the first inequality shows that the error bound Λ is at most $(f-1)$ times larger than the optimal error. The root-mean-square error, rms $= \sqrt{(\Delta^2 / \prod N_\kappa)}$, is hence larger than the one of an optimal product expansion by at most a factor of $\sqrt{(f-1)}$.

Note that POTFIT is variational in the sense that the rms-error decreases when the expansion orders are increased. This monotonic convergence is an important property of POTFIT.

3. Including weights

The inclusion of weights, i. e. minimizing $\Delta^2 = \sum_I (V_I - V_I^{\mathrm{app}})^2 w_I$, is often inevitable for obtaining an accurate product representation of the physically relevant part of the potential without going to high expansion orders. The inclusion of separable weights, $w_I = w_{i_1}^{(1)} \cdots w_{i_f}^{(f)}$, is very simple[68], but separable weights are not so helpful and not discussed here. The inclusion of non-separable weights unfortunately leads to complicated equations of little use. There is, however, a nice trick[14,69], which allows one to emulate non-separable weights by an iterative procedure. To this end we introduce a reference potential V^{ref} such that the weighted difference between the potential and its product representation is identical to the difference between the reference potential and the product representation

$$(V_I - V_I^{\mathrm{app}}) w_I = V_I^{\mathrm{ref}} - V_I^{\mathrm{app}} \quad . \tag{43}$$

Then one simply can potfit the reference potential to obtain a product representation, V^{app}, which is (almost) optimal with respect to the weighted sum of squared differences. Obviously, V^{ref} is given by

$$V_I^{\mathrm{ref}} = w_I V_I + (1 - w_I) V_I^{\mathrm{app}} \quad . \tag{44}$$

The definition of the reference potential depends on V^{app} which in turn depends on the reference potential. Hence, the equations must be solved iteratively. One first potfits V and evaluates the reference potential. Then the reference potential is potfitted and with the new

V^{app} a new reference potential is built. The process is iterated until some break-off criterion is satisfied.

When emulating non-separable weights we always have used a special form of the weights. The weights are set to one within the so called *relevant region* and to zero otherwise. The relevant region is usually defined by an energy criterion, i. e. it is the region where the potential is lower than some suitably chosen energy threshold. Restrictions on coordinates can be set as well when defining a relevant region. With such a definition of the weights, i. e. zero or one, Eq. (44) has a vivid interpretation. The reference potential is the original potential within the relevant region and the fitted potential otherwise. Moreover, with this choice of the weights we always observed a lowering of the weighted L^2 error with each iteration.

4. Computational effort and memory consumption

The potfit expansion was introduced to reduce the numerical labor when evaluating the integrals. Consider the computation of the matrix element $<\Phi_J|V|\Phi_L>$. Doing this integral on the primitive grid requires N^f multiplications. (Here we assume, for sake of simplicity, that all DOFs have the same number of grid points, $N_\kappa = N$.) Doing the integral with a potfit expansion requires sfN multiplications. The number of potential terms is, due to contraction, $s = m^{f-1}$, where, similar to above, $m_\kappa = m$ is assumed. The gain is hence

$$\text{gain}_{\text{CPU}} = \frac{1}{f}\left(\frac{N}{m}\right)^{f-1} \quad . \tag{45}$$

A potfit expansion does not only speed-up the calculation, it also compacts the representation of the potential leading to a much lower memory demand. The full potential consists of N^f data points, whereas a potfit expansion, Eq. (41), takes $Nm^{f-1} + Nm(f-1)$ data points. For $f > 2$ the second term is negligible in comparison with the first one, and one arrives at a memory gain

$$\text{gain}_{\text{mem}} = \left(\frac{N}{m}\right)^{f-1} \quad . \tag{46}$$

As an example let us consider a 6D problem where each DOF is represented by 25 grid points. Assuming $m=6$ ($m=5$), i. e. 7776 (3125) potfit terms after contraction, one has a CPU-gain of 209 (521), which is a quite remarkable speed-up. The potential consists of $N^f = 2.4 \times 10^8$ points and requires 1.8 GB of storage. The potfit consumes only 1.5 MB

(615 KB). A potfit representation is hence very compact. This is an important feature when turning to larger systems where the potential evaluated at the grid points ceases to fit into memory. Unfortunately POTFIT cannot solve this problem. Although a potfit representation is very compact, to arrive at this representation one has to perform sums over all grid points, see Eqs. (38,40). Hence, using today's workstations, POTFIT is limited to problems with less than 10^9 grid points, i. e. in general to systems with at most six or seven degrees of freedom. One way out of this dilemma is to switch to a (in general more approximate) n-mode representation (see section III C). One may then potfit the n-mode terms. But a further development of POTFIT, multi-grid POTFIT (MGPF), may provide a solution. MGPF, which is currently under development, is briefly discussed in the following subsection.

As discussed in section II C, MCTDH makes use of mode combination. For optimal performance one should use the same mode combinations in POTFIT as in MCTDH. The generalization to POTFIT with mode combination is obvious: f is replaced by p, N_κ becomes the particle grid size, and the SPPs operate on particles (combined modes) rather than on DOFs. With these substitutions all equations remain valid.

5. Multi-Grid POTFIT

The MGPF algorithm is developed to soften the strong exponential growth of the POT-FIT effort with dimensionality. For MGPF two sets of grids are to be defined. A fine grid with numbers of grid points N_κ, and a coarse grid with numbers of grid points n_κ. The fine grid is the one on which the subsequent MCTDH calculations are performed, the coarse grid is used to perform internal sums, e. g. when potential density matrices are computed. The coarse grid is assumed to be part of the fine grid.

As a first step the PES is potfitted on the coarse grid using $m_\kappa = n_\kappa$. The potfit is hence complete and the original potential is exactly reproduced on the coarse grid. In a following step the SPPs of this potfit are replaced by SPPs for the fine grid. To determine the latter we minimize the error

$$\sum_{I^\kappa} \sum_{\tilde{i}_\kappa} \left(V_{I^\kappa_{\tilde{i}_\kappa}} - V^{app}_{I^\kappa_{\tilde{i}_\kappa}} \right)^2 = \min \tag{47}$$

for $\kappa = 1, \ldots, f$. Quantities of the fine grid are marked by a tilde and $V^{app}_{I^\kappa_{\tilde{i}_\kappa}}$ denotes the

coarse grid potfit but with the SPPs of the κth DOF replaced with the fine grid SPPs, $\tilde{v}^{(\kappa)}_{\tilde{i}_\kappa j_\kappa}$. These SPPs are determined by the above minimization process. After some algebra one obtains

$$\tilde{v}^{(\kappa)}_{\tilde{i}_\kappa j_\kappa} = \sum_{i_\kappa, k_\kappa} \varrho^{(\kappa)'}_{\tilde{i}_\kappa i_\kappa} \varrho^{(\kappa)-1}_{i_\kappa k_\kappa} v^{(\kappa)}_{k_\kappa j_\kappa} \tag{48}$$

where $\varrho^{(\kappa)'}_{\tilde{i}_\kappa i_\kappa}$ denotes a potential density matrix where the first index runs over the coarse grid and the second over the fine grid. The internal summation is done over the coarse grid, i. e.

$$\varrho^{(\kappa)'}_{\tilde{i}_\kappa i_\kappa} = \sum_{I^\kappa} V_{I^\kappa_{\tilde{i}_\kappa}} V_{I^\kappa_{i_\kappa}} \tag{49}$$

MGPF requires fNn^{f-1} potential evaluations and additionally $2fNn^f$ multiplications. This is to be compared with POTFIT which requires N^f potential evaluations and fN^{f+1} additional operations. As the potential evaluations are usually the most time consuming part when potfitting, we compare these efforts for an example with parameters $f = 12$, $N = 25$, $n = m = 4$. The MGPF requires 1.3×10^9 potential evaluations while POTFIT takes 6×10^{16}. This demonstrates the great efficiency of MGPF.

A delicate question is the accuracy of MGPF. To partly answer it we state two results

- An MGPF potential reproduces the original potential exactly on the coarse grid points.

- If the original potential happens to be of product form with ranks which are equal or smaller than the MGPF expansion orders (i. e. coarse grid sizes), then MGPF reproduces the original potential exactly everywhere on the fine grid.

In particular the second statement is very assuring. However, in general the original potential will not be of low rank. Then both representations, POTFIT and MGPF, will include some error. For the very few tests we have done so far we observed that the MGPF rms-error is about four times larger than the POTFIT one, while using identical numbers of SPPs. This increase is tolerable considering the enormous reduction in effort provided by MGPF.

C. The n-mode representation

An n-mode representation[73–75] of a potential $V(\mathbf{q})$ is given by

$$V^{\text{app}}(\mathbf{q}) = V^{(0)} + \sum_i V^{(1)}_i(q_i) + \sum_{i<j} V^{(2)}_{ij}(q_i, q_j) + \sum_{i<j<k} V^{(3)}_{ijk}(q_i, q_j, q_k) + \cdots \tag{50}$$

24

where the series is truncated at a suitable order. The one-body terms $V_i^{(1)}(q_i)$ are cuts through the hyperspace with just one coordinate varying at a time. Similarly, the two-body terms $V_{ij}^{(2)}(q_i, q_j)$ are the cuts with two coordinates varying at a time. However, the over-counting of lower-dimensional grids embedded in higher dimensional ones must be accounted for. In detail the algorithm is as follows. A reference point $\mathbf{a}$ is chosen, usually the potential minimum or a saddle point. The symbol $\mathbf{a}^{(\kappa)}$ denotes the reference point except for the κth coordinate and $\mathbf{a}^{(\kappa,\nu)}$ has two coordinates missing. The n-mode terms are then defined as

$$V^{(0)} = V(\mathbf{a}) \tag{51}$$

$$V_i^{(1)}(q_i) = V(q_i \mathbf{a}^{(i)}) - V^{(0)} \tag{52}$$

$$V_{ij}^{(2)}(q_i, q_j) = V(q_i, q_j, \mathbf{a}^{(i,j)}) - V_i^{(1)}(q_i) - V_j^{(1)}(q_j) - V^{(0)} \tag{53}$$

$$\cdots \tag{54}$$

The n-mode representation has the useful feature that the individual terms are of low dimensionality (provided the representation is truncated at low order, four or five, say). Matrix elements of the potential can thus be done relatively easily, but for usage with MCTDH one would simply potfit the n-mode terms. A disadvantage of the n-mode representation is its strong combinatorial increase of the number of terms with order. This increase can be softened by mode combination as discussed in Ref.[76]. There it is also discussed how to use several reference points to enforce that the potential representation exhibits the full symmetry of the original potential. The most significant disadvantage of the n-mode representation, however, is the lack of an error control. Moreover, the representation is non-variational and an addition of a term will not necessarily reduce the representation error.

The n-mode representation is heavily used in time-independent quantum dynamical calculations, see e. g. Refs.[63,64,77]. Together with MCTDH this method has been used to study the dynamics of the Zundel cation[78,79] because this system is much too large to be treated with POTFIT.

IV. APPLICATIONS

Before one can start to simulate the dynamics of a system one obviously has to define a coordinate system and to set up the Hamiltonian. The latter consists of a kinetic energy operator (KEO) and a potential energy surface (PES). When normal mode coordinates are

used, the KEO is trivial (except for the often neglected vibrational angular momentum term). This explains why normal mode coordinates are so popular. However, the rectilinear normal modes coordinates often do not closely follow the internal motions of a molecule in particular if there are large amplitude motions. These motions are much better described by curvilinear coordinates, e. g. angles. The use of rectilinear coordinates may introduce strong *artificial correlations*, i. e. correlations which are entirely due to the use of unsuitable coordinates. (Consider to use Cartesian coordinates for the electron of a hydrogen atom.) The use of curvilinear coordinates, however, may lead to rather complicated expressions for the KEO. The excellent review of Gatti and Iung[65] discusses how to systematically obtain a KEO for the so called *polyspherical coordinates*.

On the other hand, obtaining an accurate PES for 9 or more internal coordinates, requires a major effort despite very impressive progress in PES fitting[80–82]. Moreover, the PES has then to be brought to product form as discussed in section III. In particular for large systems it is therefore attractive to use model Hamiltonians. The use of model Hamiltonians is very common in physics (spin-boson model, Hubbard model, etc.), less so in chemistry. However, the vibronic-coupling Hamiltonian, which will be discussed in the next section, is a very successful model in chemistry.

A.   Multidimensional non-adiabatic dynamics

The concept of a potential energy surface is one of the most fruitful concepts in theoretical chemistry. It relies on a separation between electronic and nuclear motion. Due to the large mass ratio between nuclei and electron masses, this – the Born-Oppenheimer separation – is often an excellent approximation. However, the approximation breaks down when the PES of different electronic states come close to each other or even intersect in a so called *conical intersection*[83,84]. The non-adiabatic coupling terms diverge at a conical intersection. Quantum-dynamical calculations are therefore usually performed in a diabatic representation, where the coupling is moved from the kinetic energy to the potential. The potential coupling is non-singular. The diabatic representation has another advantage, namely that the diabatic surfaces are much smoother than the adiabatic ones. This allows one to represent them by a simple *ansatz*, e. g. by harmonic potentials. This is done for the vibronic coupling model Hamiltonian[83,85], which in its quadratic form reads

Process	System	Formula	f	e	Ref.
Photo-excitation	pyrazine	$C_4H_4N_2$	24	2	86
	furan	C_4H_4O	$\underline{13}$	4	87
Photo-ionization	butatriene	$C_4H_4^+$	18	2	88
	allene	$C_3H_4^+$	15	3	89
	pentatetraene	$C_5H_4^+$	21	3	90
	benzene	$C_6H_6^+$	$\underline{13}$	5	91
	cyclopropane	$C_3H_6^+$	$\underline{14}$	4	92
	difluorobenzene	$C_6F_2H_4^+$	$\underline{10}$	5	93
	trifluoroacetonitrile	CF_3CN^+	$\underline{12}$	5	94
	phenylacetylene	$C_8H_6^+$	$\underline{24}$	4	95
	naphthalene	$C_{10}H_6^+$	$\underline{29}$	6	96
	antracene	$C_{14}H_{10}^+$	$\underline{31}$	6	96
Photo-detachment	phenide	C_6H_5	27	2	97

TABLE I: Collection of MCTDH calculations on vibronic motion in photo-excitation, -ionization, and -detachment spectra. The columns f and e give the numbers of DOFs and electronic states, respectively, included in the simulation. An underlined number of DOFs indicates that not all $(3N-6)$ DOFs are accounted for (reduced dimensionality calculations).

$$
\mathbf{H}_{\mathrm{dia}} = \mathbf{T}(\mathbf{q})\mathbf{1} \; + \; \sum_{i=1}^{f} \frac{\omega_i^2}{2} \begin{pmatrix} 1 & 0 \\ 0 & 1 \end{pmatrix} q_i^2 \; + \; \begin{pmatrix} \epsilon_1 & 0 \\ 0 & \epsilon_2 \end{pmatrix}
$$

$$
+ \sum_{i \in G_1} \begin{pmatrix} \kappa_i^{(1)} & 0 \\ 0 & \kappa_i^{(2)} \end{pmatrix} q_i \; + \; \sum_{(i,j) \in G_2} \begin{pmatrix} \gamma_{i,j}^{(1)} & 0 \\ 0 & \gamma_{i,j}^{(2)} \end{pmatrix} q_i q_j
$$

$$
+ \sum_{i \in G_3} \begin{pmatrix} 0 & \lambda_i \\ \lambda_i & 0 \end{pmatrix} q_i \; + \; \sum_{(i,j) \in G_4} \begin{pmatrix} 0 & \mu_{i,j} \\ \mu_{i,j} & 0 \end{pmatrix} q_i q_j \quad . \tag{55}
$$

The sets $G_1 \cdots G_4$ are determined by group theory. In the linear vibronic coupling model the bi-linear coupling terms γ and μ are ignored. The ω_i and q_i are the ground-state normal

mode frequencies and the frequency and mass scaled normal mode coordinates, respectively, and $\mathbf{T}$ denotes the KEO, which in this case is just a sum of frequency weighted second derivatives. The model parameters are determined by comparing the model to *ab-initio* calculations. The potential matrix is diagonalized and the thus obtained adiabatic model surfaces are fitted to *ab-initio* points.

The vibronic coupling Hamiltonian is a very fruitful and frequently used model[84]. As the Hamiltonian is of product form, it is very suitable for MCTDH. The photo-ionization or photo-excitation spectra of several vibronically coupled systems have been investigated with MCTDH, an (incomplete) list of these studies is given by Table I.
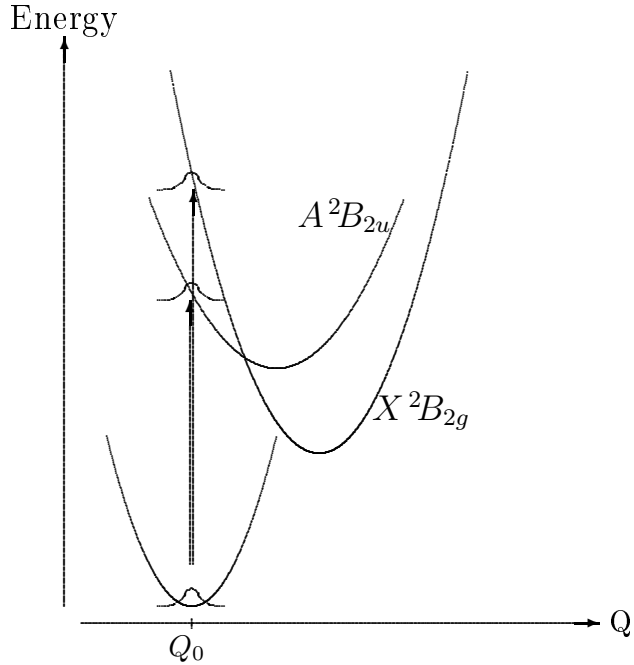
FIG. 2: Sketch of excitation in butatriene.

Let us discuss two examples, the photo-ionization of butatriene[85,88] and the photo-excitation of pyrazine[86]. The relevant electronic states of butatriene are sketched in Fig. 2. The ionization process places the ground state wave packet on one of the two coupled electronic states (Condon approximation). The wave packet is then propagated and the absorption spectrum is given by a Fourier transform of the autocorrelation function $a(t) = \langle \Psi(0) | \Psi(t) \rangle$. The resulting spectrum is shown in Fig. 3. There is a simple interpretation. The lines near 9.3 eV originate from a population of the lower ionic state and the

intensity near 10 eV is due to population of the higher one. But why is there intensity in the middle? This structure was called the *mystery band*. It was shown in 1977 by Cederbaum *et. al.* that the mystery band is due to vibronic coupling, i. e. to a break-down of the Born-Oppenheimer picture. There are many so called *vibronic* states which are electronically a mixture of both states $X\ ^2B_{2g}$ and $A\ ^2B_{2u}$. Nuclear and electronic motion can no longer be treated separately. However, the vibronic coupling is not very strong for this molecule, the spectrum is structured and resembles a progression of lines, although a closer analysis[88] shows that the several vibronic states contribute to each peak of the spectrum. Fig. 3 shows the experimental spectrum in red. Because the measurement is not absolute, the two spectra are normalized at their maxima. The MCTDH calculations[88] are converged and differences between computed and measured spectra must be attributed to the vibronic-coupling potential model. The agreement between theory and experiment is very good considering the complexity of the dynamics and the simplicity of the Hamiltonian model.
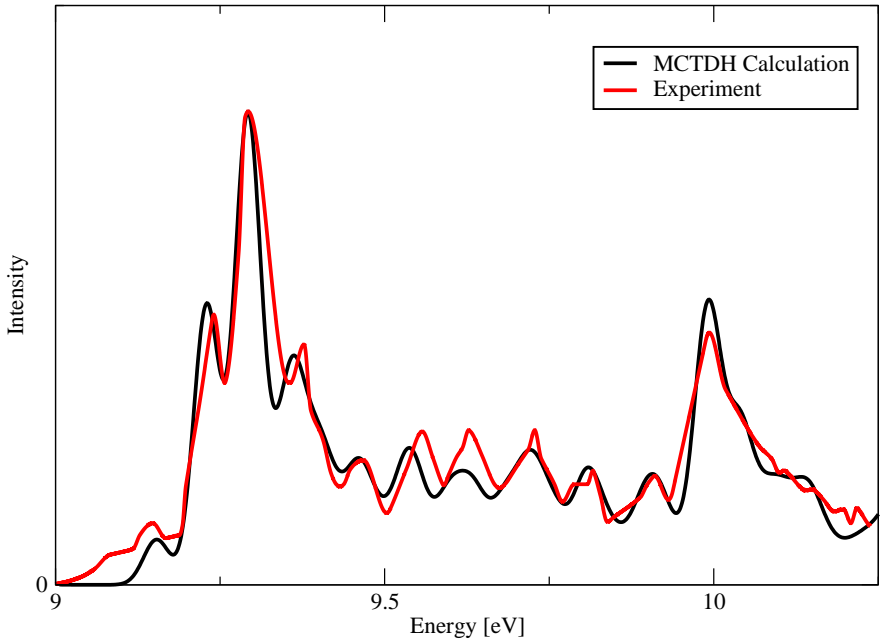
FIG. 3: Photoionization spectrum of butatriene. The black line depicts the simulation[88], and the red line shows the experiment[98].

We turn to our second example, photo-excitation of pyrazine into a vibronically coupled manifold of the S_1 and S_2 diabatic states. The dynamics is very different compared to butatriene because the vibronic coupling is rather strong and most of the vibrational

29

structures are washed out. Fig. 4, black line, shows the absorption spectrum of pyrazine. At low energies one can observe some resolved lines. These refer to vibrational states on the S_1 state. But above 2.1 eV there is only a broad, almost structure-less peak. This is a quasi-continuum of lines, even high resolution measurements have not been able to resolve individual lines. Virtually all 24 vibrational degrees of freedom are excited when the wave packet changes the electronic state in the vicinity of the conical intersection, leading to an enormously dense spectrum. The agreement with experiment[99] (see Fig. 5) is excellent.
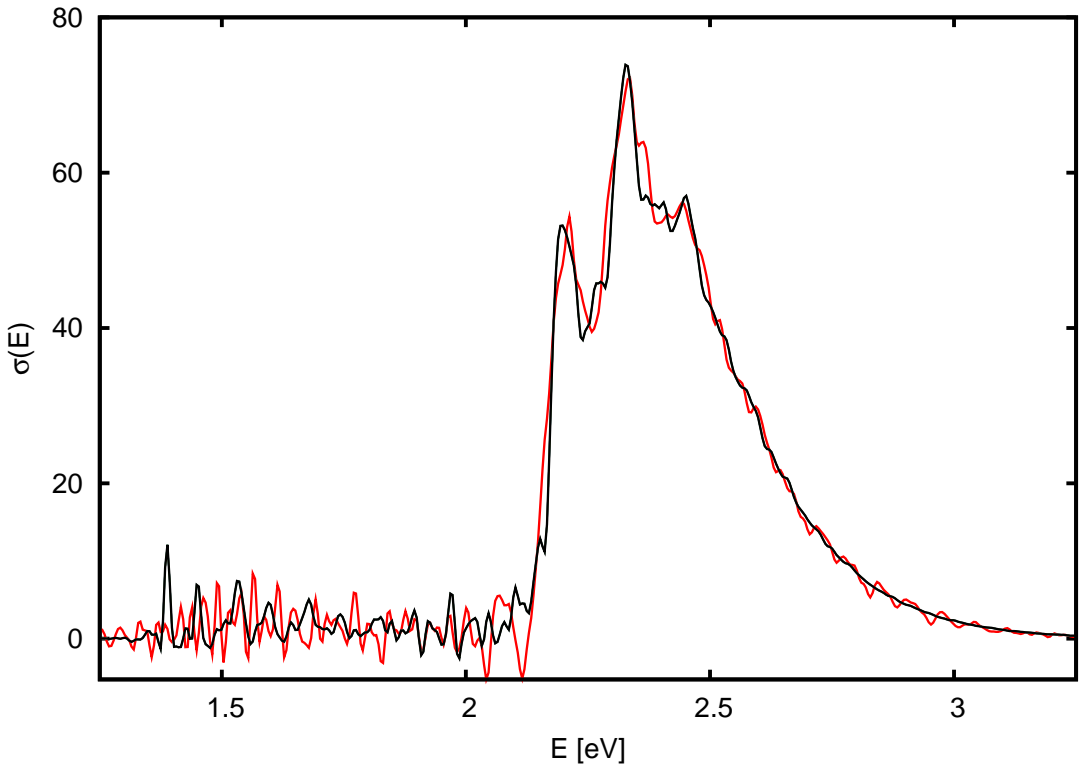
FIG. 4: Photoabsorption spectrum of pyrazine. The black line is the result of a very accurate MCTDH calculation and the red line shows a spectrum generated by a very cheap ML-MCTDH calculation. See text. The spectra shown are with respect to the energy zero-point of the Hamiltonian. To compare with experiment they must be shifted to higher energy by 2.48 eV.

The red line in Fig. 4 shows the result of an ML-MCTDH calculation[44]. The ML-MCTDH spectrum shows some artificial oscillations in the high energy tail of the spectrum (above 2.5 eV), there are some deviations in the peak structure between 2.2 eV and 2.5 eV, and the low energy part, which however is of lesser interest, is not well reproduced. But the less

Pyrazine - full 24 dimensional model
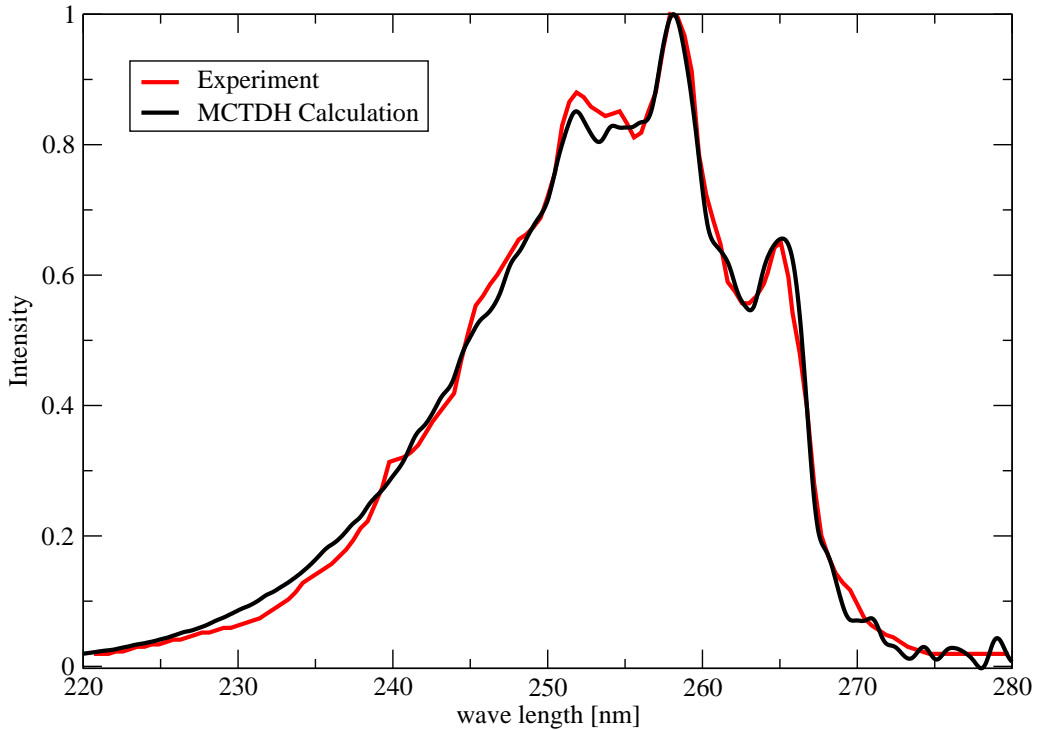
FIG. 5: Comparison experiment/MCTDH. Note that here, in contrast to Fig. 4, the photoabsorption spectrum is plotted versus wavelength rather than energy.

accurate ML-MCTDH calculation is much faster. The very accurate MCTDH calculation used a wave function with 11 million coefficients and its propagation took 630 hours on a single processor CPU. (This is an extrapolated time, the actual calculation was done on 8 cores in parallel). The ML-MCTDH wave function was described by only 22 thousand coefficients and the propagation took only 7 minutes! This demonstrates the enormous efficiency of ML-MCTDH in particular when low accuracy is sufficient. Of course, one can also perform highly accurate calculations with ML-MCTDH, but then they become costly. For more details see Ref.[44].

To detail the two calculations we show in Figs. 6, 7 the tree structures of the MCTDH and ML-MCTDH calculations, respectively. The numbers close to the lines indicate how many SPFs or grid-points are used. As the MCTDH calculation uses the multi-set formalism, there are two numbers specifying the numbers of SPFs on each of the two coupled electronic
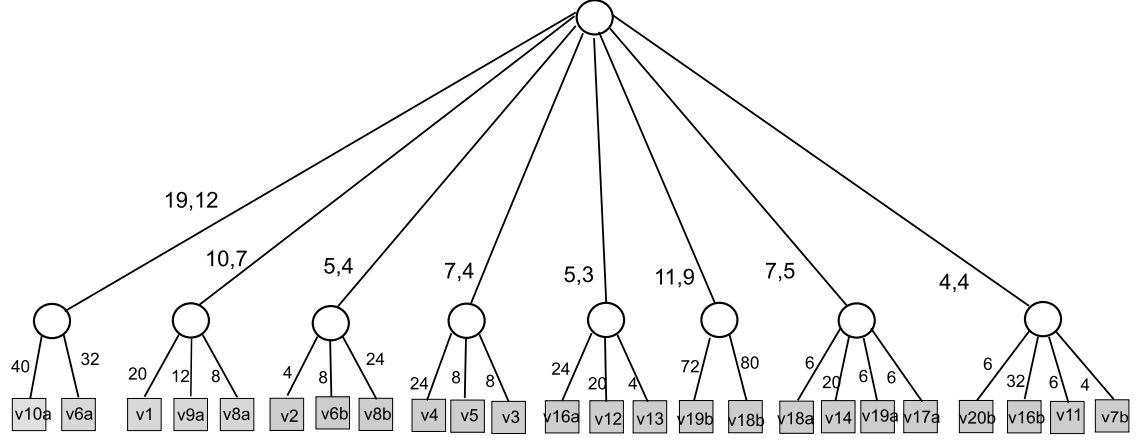
FIG. 6: MCTDH tree for pyrazine. The numbers indicate the numbers of SPFs and grid-points used. As a multi-set approach is used there are two entries for each set of combined SPFs, one for S_1 and the other for S_2.
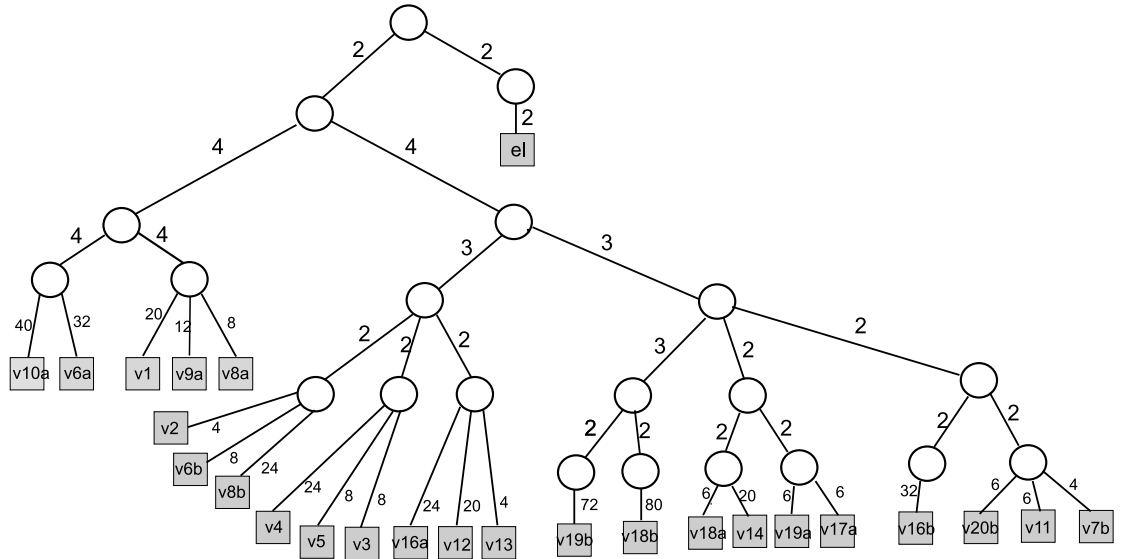

FIG. 7: ML-MCTDH tree of pyrazine. The numbers of SPFs and grid-points used are indicated.

states. ML-MCTDH calculations must be done in single-set formulation. Electronic and nuclear motions are then separated in the uppermost layer and the next layer separates the five most important DOFs ('system') from the rest ('bath'). Both parts are then further split into deeper layers, using four layers for the 'system' and up to six layers for the 'bath'.

B. IR-spectrum of the Zundel cation $H_5O_2^+$

As a final example we discuss the infra-red (IR) absorption spectrum of the Zundel cation $H_5O_2^+$. This cation is the smallest protonated water cluster and plays an important role in the proton transport in water. Although this cation is smaller (7 atoms, 15D) than pyrazine (10 atoms, 24D), and its dynamics evolves on the Born-Oppenheimer ground state surface alone, it is much harder to investigate. Firstly one has to define an appropriate set of coordinates and derive the KEO for it, and secondly the PES has to be brought to product form.
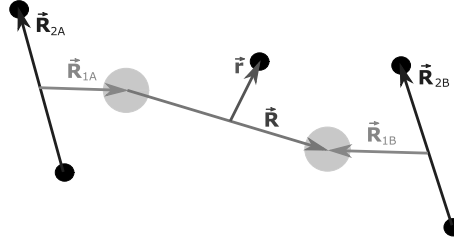

FIG. 8: Polyspherical coordinate system of $H_5O_2^+$. The vectors are parameterized by their lengths and spherical angles. The two big circles represent oxygen atoms while the small circles represent hydrogens.

The Zundel cation is a floppy molecule exhibiting anharmonic and large amplitude motions. The simple rectilinear normal mode coordinates are unsuitable, because their use introduces strong artificial correlation, i. e. correlations which can be avoided when using appropriate coordinates. We have used polyspherical[65] coordinates. These are defined by a set of internal vectors which finally are described by their lengths and spherical angles. The set of vectors used is shown in Fig. 8. The KEO for this set of coordinates is given by a very complicated and lengthy expression[78,79], and its derivation was a major part of the Zundel project[62,76,78,79,100–102].

There have been enormous advantages in potential surface fitting[80–82], and we have used

the full dimensional PES of Huang, Braams, and Bowman[103]. But a direct use of the PES is impossible because the underlying primitive product grid consists of more than 2.6×10^{15} points. As discussed in section III one cannot potfit such a large PES, one has to turn to an n-mode representation. We have generated an n-mode representation in combined modes taking all first and second order terms and three selected third order terms into account. Note that by order we refer here to order in combined modes, the DOF order goes up to 7. Furthermore, to ensure that the approximated potential has the full symmetry, 10 reference points – the 8 equivalent potential minima and the two saddle points – have been used. The n-mode terms are then potfitted to arrive at a PES in product form. For more details see Refs.[78,79].

Having derived the KEO and a compact form of the PES we turn to the MCTDH calculations. First the ground state was computed by improved relaxation. Then this wave function was multiplied with the dipole surface and the dipole operated wave packet was used as initial state for propagation. The autocorrelation function of this propagation was then Fourier transformed to obtain the IR absorption spectrum. This spectrum is shown in Fig. 9 in comparison with experimental results. Because one cannot have a dense gas of ions, direct IR absorption spectroscopy is impossible for ions. The vibrational predissociation technique was hence used. When the molecular ion absorbs a photon an attached rare gas atom is boiled off and the effect is detected by mass spectroscopy.

The agreement between theory and experiment is excellent considering the complexity of the system. The double line structure near 1000 cm^{-1}, which was a mystery for some time, could be explained. The proton motion along the O-O axis and a combination of a two phonon wagging and O-O stretching are pairs of a Fermi resonance[62,76]. The proton motion obviously creates the largest change in the dipole moment and acquires the largest oscillator strength. Due to the Fermi resonance it loans some intensity to the mentioned combination line. Similarly, the ungerade water bending line, which appears around 1750 cm^{-1}, acquires most of its intensity from coupling to the central proton motion[79].

The effect of isotopic substitution was also investigated. Fig. 10 shows the spectra of $H(H_2O)_2^+$, $D(D_2O)_2^+$, $H(D_2O)_2^+$, and $D(H_2O)_2^+$ in comparison. In the middle region, 800-2000 cm^{-1}, intensities are largely determined by Fermi resonance mixing. The resonance pattern changes due to the isotope frequency shifts, leading to unusual strong changes in intensities. The spectrum of the $D(H_2O)_2^+$ cation is the most regular one of the four. The
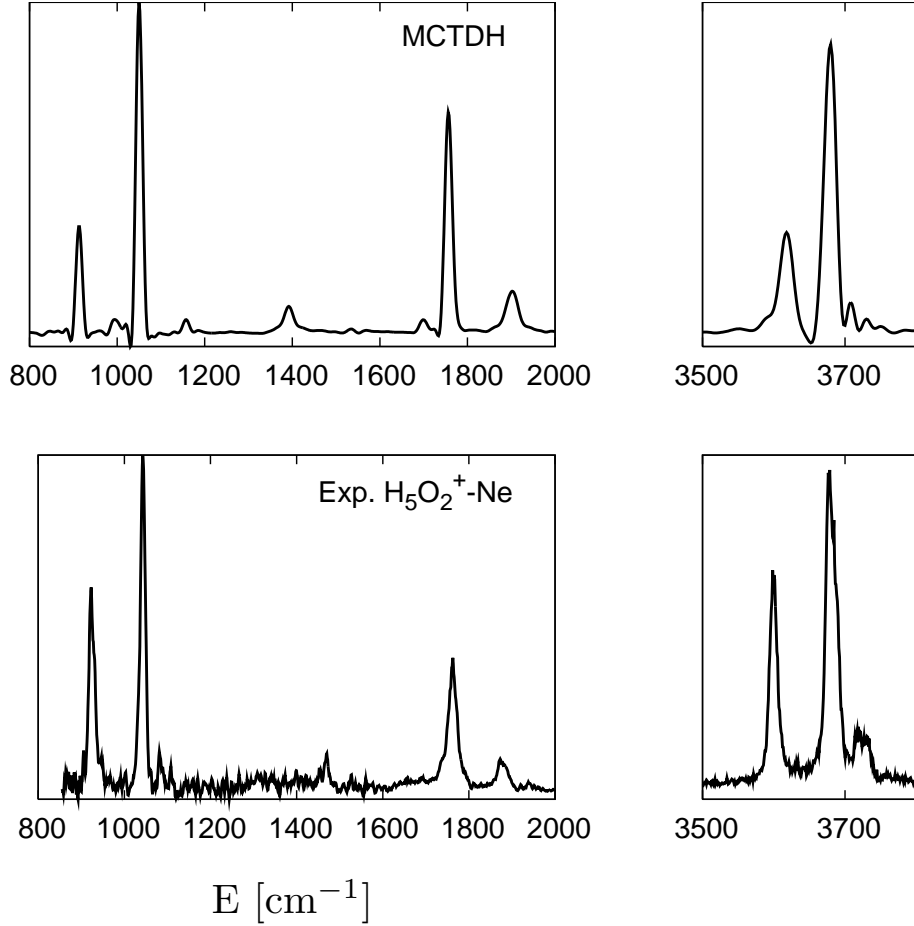
FIG. 9: Calculated IR-spectrum of of $H_5O_2^{+}$[79] (upper part) and the experimental vibrational predissociation spectrum[104] (lower part). Two different lasers are used in the experiment, which explains that there are separate figures for different energy regions. The experiment cannot detect structures below 800 cm^{-1} because the vibrational energy is then insufficient to dissociate the $H_5O_2^{+}$ – Ne van der Waals bond. The simulations show that there is indeed no absorption between 2000 and 3500 cm^{-1} and above 4000 cm^{-1}. However, there are strong lines near 100 cm^{-1} and 250 cm^{-1} (wagging motion).

combination line of the double peak, assigned as $w_3 1R$, and the water bending peak, assigned as bu, are very small. The most strongly coupled dynamics, on the other hand, is exhibited by the $H(D_2O)_2^{+}$ cation. The labels which assign the lines in Fig. 10 are explained in Ref.[102].
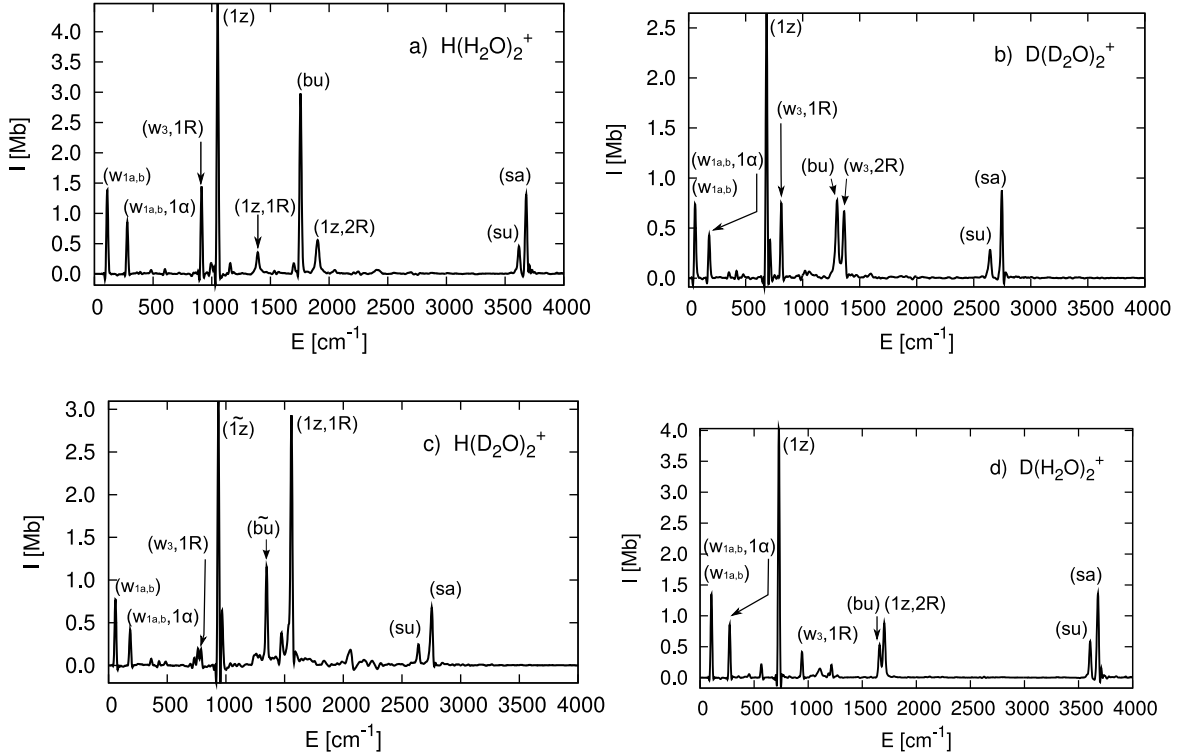
FIG. 10: IR-spectra of $H_5O_2^+$, $D_5O_2^+$, $HD_4O_2^+$, and $DH_4O_2^+$. The four isotopologues exhibit rather different spectra because the isotopic substitution changes the resonance pattern.

V. CONCLUSION

The first publication cocerning the MCTDH algorithm[12] appeared in 1990, and, in the following two decades, MCTDH has established itself as a very efficient and general algorithm for propagating wave packets. The use of a variationally determined time-dependent basis of SPFs results in an very compact wave function. Using mode combination or the multi-layer extension of MCTDH, ML-MCTDH, the wave function becomes even more compact, which allows one to treat rather large systems.

Before one can start with propagating a wavepacket, however, one must define a set of suitable coordinates, derive the KEO for this set, and develop a compact potential representation. Due to space limitations we have not discussed KEOs but refer to the excellent review of Gatti and Iung[65]. The potential representation becomes a serious problem when investigating larger systems (9D say, and larger) with a general, complicated PES. (For model systems, as exemplified by the vibronic coupling or the spin-boson models, there is no such problem.) We have therefore covered potential representations and discussed POT-

36

FIT, multi-grid POTFIT (which is still under development), and the n-mode representation. We note that a potential representation may be avoided by adopting the correlated DVR method of Manthe[105].

To demonstrate the power of the MCTDH method we have discussed two types of applications. The first type is characterized by the use of model Hamiltonians, and we have discussed the very successful vibronic coupling Hamiltonian model and used it to compute the photo-ionization spectrum of butatriene and the photo-excitation spectrum of pyrazine. There are, in fact, quite a number of MCTDH applications in this field, and MCTDH was always very successful in solving the dynamics generated by a vibronic coupling Hamiltonian.

The other type of applications, exemplified here by the study of the IR-spectrum of the Zundel cation $H_5O_2^+$, is characterized by the use of curvilinear coordinates, complicated kinetic energy operators, and a general PES which must be transformed to compact product form. Here again, MCTDH could show its great power. The very anharmonic, flexible, and strongly coupled cation exhibits a rather complicated absorption spectrum which could be explained and assigned.

MCTDH, being a very general method, has been applied to a wide range of problems. In addition to the above mentioned types of applications, it has been used to investigate reactive scattering[106–109], inelastic scattering[110,111], scattering of molecules off surfaces[112–114], isomerisation and IVR[67,115], control[116–118], nuclear motion during electron scattering or auto-ionization processes[119–121], and other problems.

A complicated algorithm like MCTDH is difficult to implement and its use involves many nuances. To bring MCTDH to success we have developed the Heidelberg MCTDH package which is available on request. See http://mctdh.uni-hd.de. The package, which comes with a comprehensive documentation, is used by several groups around the world.

VI.   ACKNOWLEDGMENTS

---

[1] J. M. Bowman, T. Carrington Jr., and H.-D. Meyer. Variational quantum approaches for computing vibrational energies of polyatomic molecules. *Mol. Phys.* **106** (2008), 2145–2182.

[2] S. Heislbetz and G. Rauhut. Vibrational multiconfiguration self-consistent field theory: Implementation and test calculations. *J. Chem. Phys.* **132** (2010), 124102.

[3] P. Seidler, M. Sparta, and O. Christiansen. Vibrational coupled cluster response theory: A general implementation. *J. Chem. Phys.* **134** (2011), 054119.

[4] E. Matyus, J. Simunek, and A. G. Csaszar. On the variational computation of a large number of vibrational energy levels and wave functions for medium-sized molecules. *J. Chem. Phys.* **131** (2009), 074106.

[5] S. G. Ramesh and E. L. Sibert. Combination of perturbative and variational methods for calculating molecular spectra: Calculation of the ν=3-5 ch stretch overtone spectrum of chf3. *J. Chem. Phys.* **103** (2006), 114307.

[6] A. Virshup, C. Punwong, T. Pogorelov, B. Lindquist, C. Ko, and T. Martinez. Photodynamics in complex environments: Ab initio multiple spawning quantum mechanical/molecular mechanical dynamics. *J. Phys. Chem. B* **113** (2009), 3280.

[7] R. Kosloff. Time-dependent quantum-mechanical methods for molecular dynamics. *J. Phys. Chem.* **92** (1988), 2087.

[8] R. Marquardt, M. Quack, I. Thanopoulos, and D. Luckhaus. Tunneling dynamics of the NH chromophore in NHD_2 during and after coherent infrared excitation. *J. Chem. Phys.* **118** (2003), 643–658.

[9] G. A. Worth, M. H. Beck, A. Jäckle, and H.-D. Meyer. The MCTDH Package, Version 8.2, (2000). H.-D. Meyer, Version 8.3 (2002), Version 8.4 (2007). See http://mctdh.uni-hd.de/.

[10] J. C. Light. Discrete variable representations in quantum dynamics. In *Time-Dependent Quantum Molecular Dynamics* (New York, 1992), J. Broeckhove and L. Lathouwers, Eds.,

Plenum, pp. 185–199.

[11] J. C. Light and T. Carrington Jr. Discrete variable representations and their utilization. *Adv. Chem. Phys.* **114** (2000), 263–310.

[12] H.-D. Meyer, U. Manthe, and L. S. Cederbaum. The multi-configurational time-dependent Hartree approach. *Chem. Phys. Lett.* **165** (1990), 73–78.

[13] U. Manthe, H.-D. Meyer, and L. S. Cederbaum. Wave-packet dynamics within the multiconfiguration Hartree framework: General aspects and application to NOCl. *J. Chem. Phys.* **97** (1992), 3199–3213.

[14] M. H. Beck, A. Jäckle, G. A. Worth, and H.-D. Meyer. The multi-configuration time-dependent Hartree (MCTDH) method: A highly efficient algorithm for propagating wave packets. *Phys. Rep* **324** (2000), 1–105.

[15] H.-D. Meyer and G. A. Worth. Quantum molecular dynamics: Propagating wavepackets and density operators using the multiconfiguration time-dependent Hartree (MCTDH) method. *Theor. Chem. Acc.* **109** (2003), 251–267.

[16] H.-D. Meyer, F. Gatti, and G. A. Worth, Eds. *Multidimensional Quantum Dynamics: MCTDH Theory and Applications.* Wiley-VCH, Weinheim, 2009.

[17] M. H. Beck and H.-D. Meyer. An efficient and robust integration scheme for the equations of motion of the multiconfiguration time-dependent Hartree (MCTDH) method. *Z. Phys. D* **42** (1997), 113–129.

[18] U. Manthe. On the integration of the multi-configurational time-dependent Hartree (MCTDH) equations of motion. *Chem. Phys.* **329** (2006), 168–178.

[19] A. D. Hammerich, U. Manthe, R. Kosloff, H.-D. Meyer, and L. S. Cederbaum. Time-dependent photodissociation of methyl iodide with five active modes. *J. Chem. Phys.* **101** (1994), 5623.

[20] J.-Y. Fang and H. Guo. Multiconfiguration time-dependent hartree studies of the CH_3I/MgO photodissociation dynamics. *J. Chem. Phys.* **101** (1994), 5831–5840.

[21] G. A. Worth, H.-D. Meyer, and L. S. Cederbaum. The effect of a model environment on the S_2 absorption spectrum of pyrazine: A wavepacket study treating all 24 vibrational modes. *J. Chem. Phys.* **105** (1996), 4412.

[22] S. Zöllner, H.-D. Meyer, and P. Schmelcher. Correlations in ultracold trapped few-boson systems: Transition from condensation to fermionization. *Phys. Rev. A* **74** (2006), 063611.

[23] S. Zöllner, H.-D. Meyer, and P. Schmelcher. Tunneling dynamics of a few bosons in a double

well. *Phys. Rev. A* **78** (2008), 013621.

[24] S. Zöllner, H.-D. Meyer, and P. Schmelcher. Composite fermionization of one-dimensional bose-bose mixtures. *Phys. Rev. A* **78** (2008), 013629.

[25] S. Zöllner, H.-D. Meyer, and P. Schmelcher. Few-boson dynamics in double wells: From single-atom to correlated pair tunneling. *Phys. Rev. Lett.* **100** (2008), 040401.

[26] A. U. J. Lode, A. I. Streltsov, O. E. Alon, H.-D. Meyer, and L. S. Cederbaum. Corrigendum: Exact decay and tunneling dynamics of interacting few boson systems. *J. Phys. B* **43** (2010), 029802.

[27] L. Pitaevskii and S. Stringari. *Bose-Einstein Condensation.* Oxford University Press, Oxford, 2003.

[28] C. J. Pethick and H. Smith. *Bose-Einstein Condensation in Dilute Gases.* Cambridge University Press, Cambridge, 2002.

[29] O. E. Alon, A. I. Streltsov, and L. S. Cederbaum. Multiconfigurational time-dependent Hartree method for bosons: Many-body dynamics of bosonic systems. *Phys. Rev. A* **77** (2008), 033613.

[30] A. I. Streltsov, O. E. Alon, , and L. S. Cederbaum. General variational many-body theory with complete self-consistency for trapped bosonic systems. *Phys. Rev. A* **73** (2006), 063626.

[31] O. E. Alon, A. I. Streltsov, and L. S. Cederbaum. Unified view on multiconfigurational time propagation for systems consisting of identical particles. *J. Chem. Phys.* **127** (2007), 154103.

[32] K. Sakmann, A. I. Streltsov, O. E. Alon, and L. S. Cederbaum. Exact quantum dynamics of a Bosonic Josephson Junction. *Phys. Rev. Lett.* **103** (2009), 2206011.

[33] J. Zanghellini, M. Kitzler, C. Fabian, T. Brabec, and A. Scrinzi. An MCTDHF approach to multi–electron dynamics in laser fields. *Laser Phys.* **13** (2003), 1064.

[34] T. Kato and H. Kono. Time-dependent multiconfiguration theory for electronic dynamics of molecules in an intense laser field. *Chem. Phys. Lett.* **392** (2004), 533.

[35] M. Nest, T. Klamroth, and P. Saalfrank. The multiconfiguration time-dependent Hartree-Fock method for quantum chemical calculations. *J. Chem. Phys.* **122** (2005), 124102.

[36] M. Nest, R. Padmanaban, and P. Saalfrank. Time-dependent approach to electronically excited states of molecules with the multiconfiguration time-dependent Hartree-Fock method. *J. Chem. Phys.* **126** (2007), 214106.

[37] J. Caillat, J. Zanghellini, M. Kitzler, O. Koch, W. Kreuzer, and A. Scrinzi. Correlated multielectron systems in strong laser fields - an mctdhf approach. *Phys. Rev. A* **71** (2005),

012712.

38 G. Jordan and A. Scrinzi. Core-polarization effects in molecular high harmonic generation. *New J. Phys.* **10** (2008), 025035.

39 S. Sukiasyan, C. McDonald, C. Destefani, M. Y. Ivanov, and T. Brabec. Multielectron correlation in high-harmonic generation: A 2D model analysis. *Phys. Rev. Lett.* **102** (2009), 223002.

40 D. J. Haxton, K. V. Lawler, and C. W. McCurdy. Multiconfiguration time-dependent Hartree-Fock treatment of electronic and nuclear dynamics in diatomic molecules. *Phys. Rev. A* **83** (2011), 063416.

41 H. Wang and M. Thoss. Multilayer formulation of the multiconfiguration time-dependent Hartree theory. *J. Chem. Phys.* **119** (2003), 1289–1299.

42 U. Manthe. A multilayer multiconfigurational time-dependent hartree approach for quantum dynamics on general potential energy surfaces. *J. Chem. Phys.* **128** (2008), 164116.

43 U. Manthe. Layered discrete variable representations and their application within the multiconfigurational time-dependent hartree approach. *J. Chem. Phys.* **130** (2009), 054109.

44 O. Vendrell and H.-D. Meyer. Multilayer multiconfiguration time-dependent Hartree method: Implementation and applications to a Henon-Heiles Hamiltonian and to pyrazine. *J. Chem. Phys.* **134** (2011), 044135.

45 H. Wang and M. Thoss. Quantum-mechanical evaluation of the Boltzmann operator in correlation functions for large molecular systems: A multilayer multiconfiguration time-dependent Hartree approach. *J. Chem. Phys.* **124** (2006), 034114.

46 H. Wang and M. Thoss. Quantum dynamical simulation of electron-transfer reactions in an anharmonic environment. *J. Phys. Chem. A* **111** (2007), 10369.

47 M. Thoss and H. Wang. Quantum dynamical simulation of ultrafast molecular processes in the condensed phase. *Chem. Phys.* **322** (2006), 210.

48 M. Thoss, I. Kondov, and H. Wang. Correlated electron-nuclear dynamics in ultrafast photoinduced electron-transfer reactions at dye-semiconductor interfaces. *Phys. Rev. B* **76** (2007), 153331.

49 I. Kondov, M. Thoss, and H. Wang. Quantum dynamics of photoinduced electron transfer reactions in dye-semiconductor systems: Description and application to coumarin 343-TiO$_2$. *J. Phys. Chem. C* **111** (2007), 11970–11981.

[50] H. Wang and M. Thoss. From coherent motion to localization: dynamics of the spin-boson model at zero temperature. *New J. Phys.* **10** (2008), 115005.

[51] H. Wang and M. Thoss. From coherent motion to localization: II. Dynamics of the spin-boson model with sub-Ohmic spectral density at zero temperature. *Chem. Phys.* **370** (2010), 78 – 86.

[52] H. Wang and M. Thoss. Numerically exact quantum dynamics for indistinguishable particles: The multilayer multiconfiguration time-dependent Hartree theory in second quantization representation. *J. Chem. Phys.* **131**, 2 (2009), 024114.

[53] R. Kosloff and H. Tal-Ezer. A direct relaxation method for calculating eigenfunctions and eigenvalues of the Schrödinger equation on a grid. *Chem. Phys. Lett.* **127** (1986), 223.

[54] H.-D. Meyer, F. Le Quéré, C. Léonard, and F. Gatti. Calculation and selective population of vibrational levels with the Multiconfiguration Time-Dependent Hartree (MCTDH) algorithm. *Chem. Phys.* **329** (2006), 179–192.

[55] K. Drukker and S. Hammes-Schiffer. An analytical derivation of MC-SCF vibrational wave functions for the quantum dynamical simulation of multiple proton transfer reactions: Initial application to protonated water chains. *J. Chem. Phys.* **107** (1997), 363.

[56] F. Culot and J. Liévin. A multiconfigurational SCF computational method for the resolution of the vibrational Schrödinger equation in polyatomic molecules. *Theor. Chem. Acc.* **89** (1994), 227.

[57] F. Culot, F. Laruelle, and J. Liévin. A vibrational CASSCF study of stretch-bend interactions and their influence on infrared intensities in the water molecule. *Theor. Chem. Acc.* **92** (1995), 211.

[58] J. Hinze. MC-SCF. I. The multi-configuration self-consistent-field method. *J. Chem. Phys.* **59** (1973), 6424.

[59] E. Davidson. The iterative calculation of a few of the lowest eigenvalues and corresponding eigenvectors of large real-symmetric matrices. *J. Comp. Phys.* **17** (1975), 87.

[60] L. J. Doriol, F. Gatti, C. Iung, and H.-D. Meyer. Computation of vibrational energy levels and eigenstates of fluoroform using the multiconfiguration time-dependent Hartree method. *J. Chem. Phys.* **129** (2008), 224109.

[61] F. Richter, F. Gatti, C. Léonard, F. Le Quéré, and H.-D. Meyer. Time–dependent wave packet study on trans–cis isomerisation of HONO driven by an external field. *J. Chem. Phys.* **127**

(2007), 164315.

[62] O. Vendrell, F. Gatti, and H.-D. Meyer. Full dimensional (15D) quantum-dynamical simulation of the protonated water dimer II: Infrared spectrum and vibrational dynamics. *J. Chem. Phys.* **127** (2007), 184303.

[63] J. M. Bowman, S. Carter, and X. Huang. MULTIMODE: a code to calculate rovibrational energies of polyatomic molecules. *Int. Rev. Phys. Chem.* **22** (2003), 533–549.

[64] M. Neff and G. Rauhut. Toward large scale vibrational configuration interaction calculations. *J. Chem. Phys.* **131**, 12 (2009), 124129.

[65] F. Gatti and C. Iung. Exact and constrained kinetic energy operators for polyatomic molecules: The polyspherical approach. *Phys. Rep.* **484** (2009), 1–69.

[66] F. Richter, M. Hochlaf, P. Rosmus, F. Gatti, and H.-D. Meyer. A study of mode–selective trans–cis isomerisation in HONO using ab initio methodology. *J. Chem. Phys.* **120** (2004), 1306–1317.

[67] F. Richter, P. Rosmus, F. Gatti, and H.-D. Meyer. Time–dependent wavepacket study on trans–cis isomerisation of HONO. *J. Chem. Phys.* **120** (2004), 6072–6084.

[68] A. Jäckle and H.-D. Meyer. Product representation of potential energy surfaces. *J. Chem. Phys.* **104** (1996), 7974.

[69] A. Jäckle and H.-D. Meyer. Product representation of potential energy surfaces II. *J. Chem. Phys.* **109** (1998), 3772.

[70] L. D. Lathauwer, B. D. Moor, and J. Vandewalle. A multilinear singular value decomposition. *SIAM Journal on Matrix Analysis and Applications* **21**, 4 (2000), 1253–1278.

[71] L. D. Lathauwer, B. D. Moor, and J. Vandewalle. On the best rank-1 and rank-$(R_1,R_2,\ldots,R_N)$ approximation of higher-order tensors. *SIAM Journal on Matrix Analysis and Applications* **21**, 4 (2000), 1324–1342.

[72] E. Schmidt. Zur Theorie der linearen und nichtlinearen Integralgleichungen. *Math. Ann.* **63** (1906), 433.

[73] J. O. Jung and R. B. Gerber. Vibrational wave functions and spectroscopy of $(H_2O)_n$, $n = 2, 3, 4, 5$: Vibrational self-consistent field with correlation corrections. *J. Chem. Phys.* **105** (1996), 10332.

[74] S. Carter, S. J. Culik, and J. M. Bowman. Vibrational self-consistent field method for many-mode systems: A new approach and application to the vibrations of CO adsorbed on Cu(100).

J. Chem. Phys. **107** (1997), 10458.

[75] G. Li, S. Wang, C. Rosenthal, and H. Rabitz. High dimensional model representations generated from low dimensional data samples. 1. mp-cut-hdmr. *J. Math. Chem.* **30** (2001), 1–30.

[76] O. Vendrell, F. Gatti, and H.-D. Meyer. Dynamics and infrared spectroscopy of the protonated water dimer. *Angew. Chem. Int. Ed.* **46** (2007), 6918–6921.

[77] J. M. Bowman, X. Huang, N. C. Handy, and S. Carter. Vibrational levels of methanol calculated by the reaction path version of MULTIMODE, using an *ab initio*, full-dimensional potential. *J. Phys. Chem. A* **111** (2007), 7317.

[78] O. Vendrell, F. Gatti, D. Lauvergnat, and H.-D. Meyer. Full dimensional (15D) quantum-dynamical simulation of the protonated water dimer I: Hamiltonian setup and analysis of the ground vibrational state. *J. Chem. Phys.* **127** (2007), 184302.

[79] O. Vendrell, M. Brill, F. Gatti, D. Lauvergnat, and H.-D. Meyer. Full dimensional (15D) quantum-dynamical simulation of the protonated water dimer III: mixed Jacobi-valence parametrization and benchmark results for the zero-point energy, vibrationally excited states and infrared spectrum. *J. Chem. Phys.* **130** (2009), 234305.

[80] B. J. Braams and J. M. Bowman. Permutationally invariant potential energy surfaces in high dimensionality. *Int. Rev. Phys. Chem.* **28** (2009), 577–606.

[81] M. A. Collins. Molecular potential energy surfaces constructed from interpolation of systematic fragment surfaces. *J. Chem. Phys.* **127** (2007), 024104.

[82] R. Dawes, D. L. Thompson, Y. Guo, A. F. Wagner, and M. Minkoff. Interpolating moving least-squares methods for fitting potential energy surfaces: Computing high-density potential energy surface data from low-density ab initio data points. *J. Chem. Phys.* **126** (2007), 184108.

[83] H. Köppel, W. Domcke, and L. S. Cederbaum. Multimode molecular dynamics beyond the Born-Oppenheimer approximation. *Adv. Chem. Phys.* **57** (1984), 59.

[84] W. Domcke, D. R. Yarkony, and H. Köppel, Eds. *Conical Intersections.* World Scientific, New Jersey, 2004.

[85] L. S. Cederbaum, W. Domcke, H. Köppel, and W. von Niessen. Strong vibronic coupling effects in ionization spectra: The "mystery band" of butatriene. *Chem. Phys.* **26** (1977), 169.

[86] A. Raab, G. Worth, H.-D. Meyer, and L. S. Cederbaum. Molecular dynamics of pyrazine after excitation to the S_2 electronic state using a realistic 24-mode model Hamiltonian. *J. Chem. Phys.* **110** (1999), 936–946.

[87] E. V. Gromov, A. B. Trofimov, N. M. Vitkovskaya, H. Köppel, J. Schirmer, H.-D. Meyer, and L. S. Cederbaum. Theoretical study of excitations in furan: Spectra and molecular dynamics. *J. Chem. Phys.* **121** (2004), 4585.

[88] C. Cattarius, G. A. Worth, H.-D. Meyer, and L. S. Cederbaum. All mode dynamics at the conical intersection of an octa-atomic molecule: Multi-configuration time-dependent Hartree (MCTDH) investigation on the butatriene cation. *J. Chem. Phys.* **115** (2001), 2088–2100.

[89] S. Mahapatra, G. A. Worth, H. D. Meyer, L. S. Cederbaum, and H. Köppel. The $\widetilde{A}^2E$ $\widetilde{B}^2B_2$ photoelectron bands of allene beyond the linear coupling scheme: An *ab initio* dynamical study including all fifteen vibrational modes. *J. Phys. Chem. A* **105** (2001), 5567–5576.

[90] A. Markmann, G. Worth, S. Mahapatra, H.-D. Meyer, H. Köppel, and L. Cederbaum. Simulation of a complex spectrum: Interplay of five electronic states and 21 vibrational degrees of freedom in $C_5H_4^+$. *J. Chem. Phys.* **123** (2005), 204310.

[91] H. Köppel, M. Döscher, I. Baldea, H.-D. Meyer, and P. G. Szalay. Multistate vibronic interactions in the benzene radical cation. II. Quantum dynamical simulations. *J. Chem. Phys.* **117** (2002), 2657–2671.

[92] T. S. Venkatesan, S. Mahapatra, H.-D. Meyer, H. Köppel, and L. S. Cederbaum. Multimode Jahn-Teller and Pseudo-Jahn-Teller interactions in the cyclopropane radical cation: Complex vibronic spectra and nonradiative decay dynamics. *J. Phys. Chem. A* **111** (2007), 1746.

[93] S. Faraji, H.-D. Meyer, and H. Köppel. Multistate vibronic interactions in difluorobenzene radical cations. II Quantum dynamical simulations. *J. Chem. Phys.* **129** (2008), 074311.

[94] T. Mondal and S. Mahapatra. Complex dynamics at conical intersections: Vibronic spectra and ultrafast decay of electronically excited trifluoroacetonitrile radical cation. *J. Phys. Chem. A* **112** (2008), 8215–8225.

[95] V. S. Reddy and S. Mahapatra. Electronic nonadiabatic interactions and ultrafast internal conversion in phenylacetylene radical cation. *J. Chem. Phys.* **130** (2009), 124303.

[96] V. S. Reddy, S. Ghanta, and S. Mahapatra. First principles quantum dynamical investigation provides evidence for the role of polycyclic aromatic hydrocarbon radical cations in interstellar physics. *Phys. Rev. Lett.* **104** (2010), 111102.

[97] V. S. Reddy, T. S. Venkatesan, and S. Mahapatra. Vibronic interactions in the photodetachment spectroscopy of phenide anion. *J. Chem. Phys.* **126** (2007), 074306.

[98] F. Brogli, E. Heilbronner, E. Kloster-Jensen, A. Schmelzer, A. S. Manocha, J. A. Pople,

and L. Radom. The photoelectron spectrum of butatriene. *Chem. Phys.* **4** (1974), 107–119.

99 I. Yamazaki, T. Murao, T. Yamanaka, and K. Yoshihara. Intramolecular electronic relaxation and photoisomerisation processes in the isolated Azabenzene molecules Pyridine, Pyrazine and Pyrimidine. *Faraday Discuss. Chem. Soc.* **75** (1983), 395.

100 O. Vendrell and H.-D. Meyer. A proton between two waters: insight from full-dimensional quantum-dynamics simulations of the $[H_2O\text{-}H\text{-}OH_2]^+$ cluster. *Phys. Chem. Chem. Phys.* **10** (2008), 4692–4703.

101 O. Vendrell, F. Gatti, and H.-D. Meyer. Strong isotope effects in the infrared spectrum of the zundel cation. *Angew. Chem. Int. Ed.* **48** (2009), 352 – 355.

102 O. Vendrell, F. Gatti, and H.-D. Meyer. Full dimensional (15D) quantum-dynamical simulation of the protonated water dimer IV: Isotope effects in the infrared spectra of $D(D_2O)_2^+$, $H(D_2O)_2^+$ and $D(H_2O)_2^+$ isotopologues. *J. Chem. Phys.* **131** (2009), 034308.

103 X. Huang, B. J. Braams, and J. M. Bowman. *Ab initio* potential energy and dipole moment surfaces for $H_5O_2^+$. *J. Chem. Phys.* **122** (2005), 044308.

104 N. I. Hammer, E. G. Diken, J. R. Roscioli, M. A. Johnson, E. M. Myshakin, K. D. Jordan, A. B. McCoy, J. M. Bowman, and S. Carter. The vibrational predissociation spectra of the $H_5O_2^+ \cdot RG_n$ (RG=Ar,Ne) clusters: Correlation of solvent perturbations in the free OH and shared proton transitions of the Zundel ion. *J. Chem. Phys.* **122** (2005), 244301.

105 U. Manthe. A time-dependent discrete variable representation for (multi-configuration) Hartree methods. *J. Chem. Phys.* **105** (1996), 6989.

106 S. Sukiasyan and H.-D. Meyer. Reaction cross section for the $H+D_2(\nu_0 = 1) \rightarrow HD+D$ and $D+H_2(\nu_0 = 1) \rightarrow DH+H$ systems. A multi-configuration time-dependent Hartree (MCTDH) wave-packet propagation study. *J. Chem. Phys.* **116** (2002), 10641–10647.

107 T. Wu, H.-J. Werner, and U. Manthe. First-principles theory for the $H + CH_4 \rightarrow H_2 + CH_3$ reaction. *Science* **306** (2004), 2227–2229.

108 R. van Harrevelt, G. Nyman, and U. Manthe. Accurate quantum calculations of the reaction rates for H/D + CH_4. *J. Chem. Phys.* **126**, 8 (2007), 084303.

109 S. Bhattacharya, A. N. Panda, and H.-D. Meyer. Multiconfiguration time-dependent Hartree approach to study the OH+H_2 reaction. *J. Chem. Phys.* **132** (2010), 214304.

110 F. Otto, F. Gatti, and H.-D. Meyer. Rotational excitations in *para*-H_2 + *para*-H_2 collisions: Full- and reduced-dimensional quantum wave packet studies comparing different potential

energy surfaces. *J. Chem. Phys.* **128** (2008), 064305.

[111] F. Otto, F. Gatti, and H.-D. Meyer. Erratum: "Rotational excitations in *para*-H_2 + *para*-H_2 collisions: Full- and reduced-dimensional quantum wave packet studies comparing different potential energy surfaces". *J. Chem. Phys.* **131** (2009), 049901.

[112] M.-C. Heitz and H.-D. Meyer. Rotational and diffractive inelastic scattering of a diatom on a corrugated surface: A multiconfiguration time-dependent Hartree (MCTDH) study on N_2/LiF(001). *J. Chem. Phys.* **114** (2001), 1382–1392.

[113] R. van Harrevelt and U. Manthe. Multiconfigurational time-dependent Hartree calculations for dissociative adsorption of H_2 on Cu(100). *J. Chem. Phys.* **121** (2004), 3829–3835.

[114] C. Crespos, H.-D. Meyer, R. C. Mowrey, and G. J. Kroes. Multiconfiguration time-dependent Hartree method applied to molecular dissociation on surfaces: H_2+Pt(111). *J. Chem. Phys.* **124** (2006), 074706.

[115] C. Iung, F. Gatti, and H.-D. Meyer. Intramolecular vibrational energy redistribution in the highly excited Fluoroform molecule: A quantum mechanical study using the MCTDH algorithm. *J. Chem. Phys.* **120** (2004), 6992–6998.

[116] L. Wang, H.-D. Meyer, and V. May. Femtosecond laser pulse control of multidimensional vibrational dynamics: Computational studies on the pyrazine molecule. *J. Chem. Phys.* **125** (2006), 014102.

[117] M. Schröder, J.-L. Carreon-Macedo, and A. Brown. Implementation of an iterative algorithm for optimal control of molecular dynamics into MCTDH. *Phys. Chem. Chem. Phys.* **10** (2008), 850.

[118] M. Schröder and A. Brown. Realization of the cnot quantum gate operation in 6d ammonia using the oct-mctdh approach. *J. Chem. Phys.* **131** (2009), 034101.

[119] D. J. Haxton, Z. Zhang, H.-D. Meyer, T. N. Rescigno, and C. W. McCurdy. Dynamics of dissociative attachment of electrons to water through the $^2B_1$ metastable state of the anion. *Phys. Rev. A* **69** (2004), 062714.

[120] D. J. Haxton, T. N. Rescigno, and C. W. McCurdy. Dissociative electron attachment to the H_2O molecule. II. Nuclear dynamics on coupled electronic surfaces within the local complex potential model. *Phys. Rev. A* **75** (2007), 012711.

[121] M. Eroms, O. Vendrell, M. Jungen, and H.-D. Meyer. Nuclear dynamics during the resonant Auger decay of water molecules. *J. Chem. Phys.* **130** (2009), 154307.

[122] Actually H_{JK} is never built but applied term by term to the A-vector.